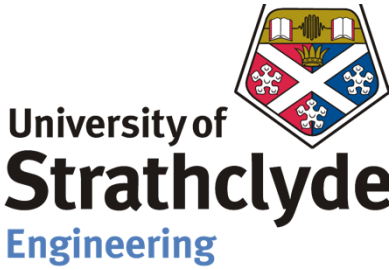

Department of Mechanical and Aerospace Engineering

Wind Turbine Decommissioning: Mechanical Assessment of Yaw Calipers for Reuse.

Author: Fraser Grant O'Neill

Supervisor: Dr Fiona Sillars

A thesis submitted in partial fulfilment for the requirement of degree in

Master of Science in Sustainable Engineering: Renewable Energy Systems and the Environment

2022

Copyright Declaration

Signed:  Date:11/08/22

Student No.20218605

Abstract

This project is part of the knowledge exchange between the University of Strathclyde and Renewable Parts Ltd. The project has focused on looking at the damage features of BSAB-S-120 calipers after service and primarily investigate reasons for fatigue damage. FEA analysis has been carried out to evaluate the design of the part against fatigue damage estimates. This has shown that under non-uniformly distributed loads the part experiences torsion leading to fatigue damage in the area reported by Renewable Parts Ltd. However, analysis has shown this area is the last location on the part to fail. Optical Microscopy and SEM was utilised to investigate the micro structure of the material at failure locations. This showed the presentence of a cast skin rich in flake graphite. Sand grains were found on the surface of the material with oxidation occurring in gaps between the surface and the grains. These factors along with surface roughness are suspected to cause fatigue cracking in this location after experiencing cyclic torsional loading. A fatigue fixture has been designed to allow fatigue testing on the part to take place so that this theory can be validated. Specimens have also been harvested from the part and machined to allow fatigue testing as per ASTM E606 to take place in an effort to create an S-N curve that will improve future analysis of the part for fatigue life estimates.

Acknowledgements

I would to thank Dr Fiona Sillars for her guidance and support throughout this project and keeping me on the correct path. Furthermore, I would like to thank James Kelly and Dr Maider Olasolo who have kindly helped me by providing their skills and knowledge within optical and scanned electron microscopy. I would likewise like to thank all the technicians at the Mechanical and Aerospace department workshop for their skills and knowledge within manufacturing and machining of test specimens.

Table of Contents

List of Figures

List of Tables

Nomenclature

Symbol	Description
a_f	Size of crack at failure
K_{IC}	Fracture toughness of the material
Y	A geometrical factor calculated from the length of the crack in divided by the width of the crack surface (a/W)
S	Stress range for the application
N_f	Number of cycles to failure
C	Material constant that is dependent on environment and residual stresses. This can be found in literature
a_o	Initial crack size at time of inspection
m	Material constant that is dependent on environment and residual stresses. This can be found in literature
S_R	Stress range for the application

1.0 Introduction

This project is part of the work between the University of Strathclyde and Renewable Parts Ltd to establish an economically and environmentally friendly approach to wind turbine maintenance through the use of refurbished parts. In June 2022 the two organisations, along with SSE Renewables, signed a Memorandum of Understanding (MoU) stating that they wish to make Scotland a hub for the advanced research and development of wind turbine components remanufacture [1]. While this is an exciting time for wind energy, many older farms are coming to the end of their life and therefore decommissioning must be looked at. It is estimated that by 2050 up to 50,000 turbines will be decommissioned resulting in 70 million tonnes of waste [2]. Renewable Parts Ltd.'s goal is to help companies reduce their carbon footprint by using their specialist knowledge to return unserviceable parts to their 'as new' condition [3]. This project hopes to add to this specialist knowledge by focusing on the mechanical assessment of the BSAB-S-120 hydraulic brake caliper. These are currently refurbished by Renewable Parts Ltd and are found on the 3.6MW Siemens Turbine variants, one of Siemens most popular turbines. Renewable Parts Ltd are seeking to gain a better understanding of the component in an effort to salvage more of these calipers and provide a better estimate of the remaining lifespan of the part. Phase 1 of the project has already been completed, which investigated the material properties and bore damage of the caliper. This is phase 2 and mainly focuses on the fatigue cracking on the part with an assessment of possible reasons for damage to other areas of the part.

1.1Aims

The aims of this project can be seen in Table 1.

Table 1: Project Aims

Project Aims	
1	Assess why failure occurs in the calipers
2	Design fatigue analysis method for calipers
3	Design fatigue testing fixture
4	Create a method for measuring fatigue of a caliper

1.2 Methodology

The project has followed the steps seen in Figure 1 in order to fulfil the project aims. At the beginning of the project, an initial literature review was conducted. Knowledge was continually gained from academic sources throughout the project represented in green. Researching into the operations and function of the calipers were looked at to better understand how damage can occur. This was followed by an analysis of offshore wind farm temperatures to understand if thermal changes could be affecting the parts. Project work started by modelling a caliper half in Creo CAD software to allow for the design of experiments and Finite Element Analysis, (FEA). This allowed for the analysis of loading conditions and how they affect the part in terms of fatigue. A fatigue experiment was also designed to evaluated the components fatigue life. Effected damage areas were harvested and analysed on a microscopic scale via optical and scanned electron microscopy. With the results of all the analysis the project findings were written up and recommendations made.

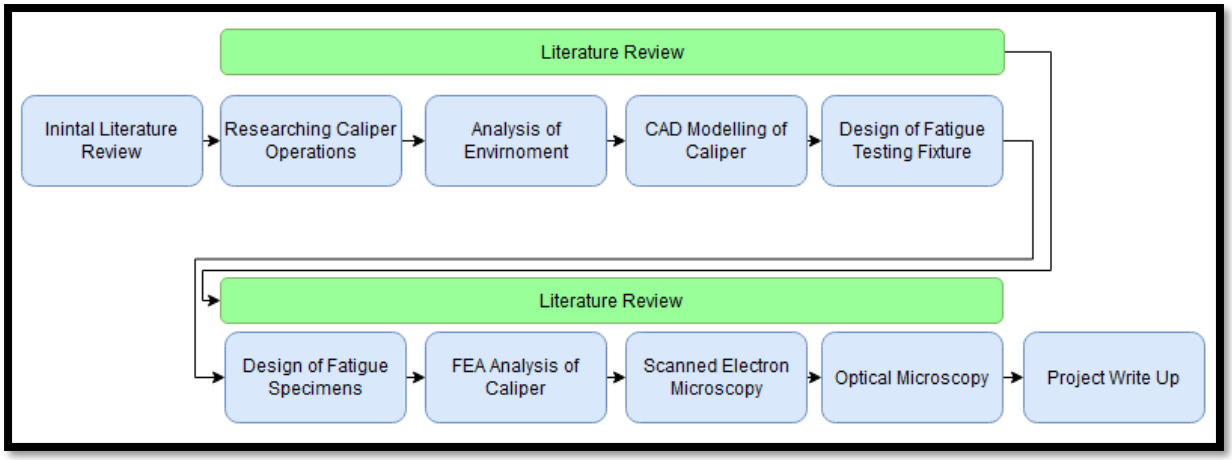

Figure 1: Project Methodology

1.3 Yaw Caliper Application

For this project the caliper investigated was a Svendborg BSAB-120-S-100 which has severed its operational life within a Siemens 3.6MW offshore wind turbine. Within the turbine there are eight sets of calipers, see Figure 2. These calipers are positioned around the yaw disc on the inside diameter and operate by applying three hydraulic pistons in the vertical direction to push a brake pad onto the surface of the yaw disc.

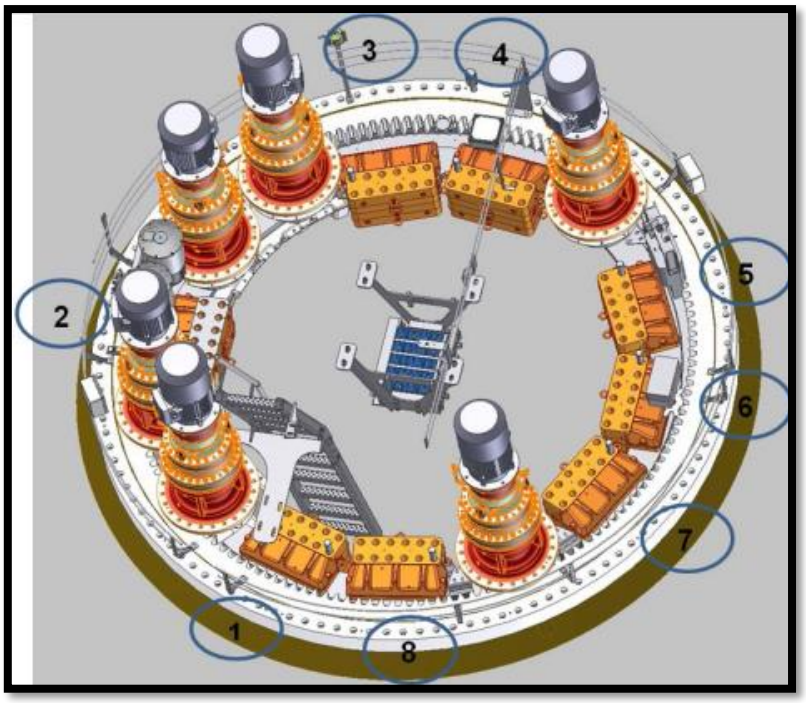

Figure 2: Yaw Caliper Position in a Siemens 3.6MW

These two halves apply a vertical clamping force, that is referred to as the breaking force, which in turn stops the yaw disc. This loading condition results in the caliper experiencing both vertical normal forces from clamping as well as tangential frictional forces from the yaw disc, see Figure 3.

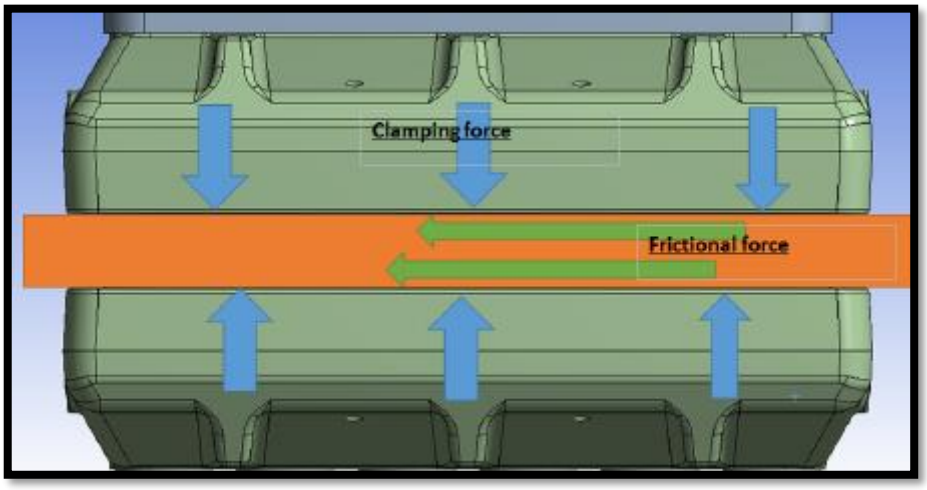

Figure 3: Loading Conditions on the Caliper [4]

1.4 Caliper Problems

The calipers have a rated operational lifetime of 1.5 million cycles. These cycles can work at a maximum of 18MPa pressure within the piston cylinders. As the lifetime of the parts come to the end of their deemed service lifetime a number of problems have been observed. These include the following:

- Fatigue cracking and in some instances fracture. A component with signs of fatigue cracking cannot be put back into service as its fatigue life is currently unknown.
- Piston cylinder damage to the cylinder walls changing these to an oval shape and causing the cylinder to no longer be concentric
- Hydraulic oil contamination which causes the oil to be very viscous and clumpy.

Fatigue cracking has been found within the cavity between the clearance holes on the ledged surface and have been identified through dye penetration, see Figure 4 & Figure 5. These cracks appear in the crested waveform shape typical of fatigue cracking. Other units have experienced fracture at these points resulting in component failure. In an operational environment this could create catastrophic failures within the turbine. As a result, this is currently the largest risk to the component going back into service.

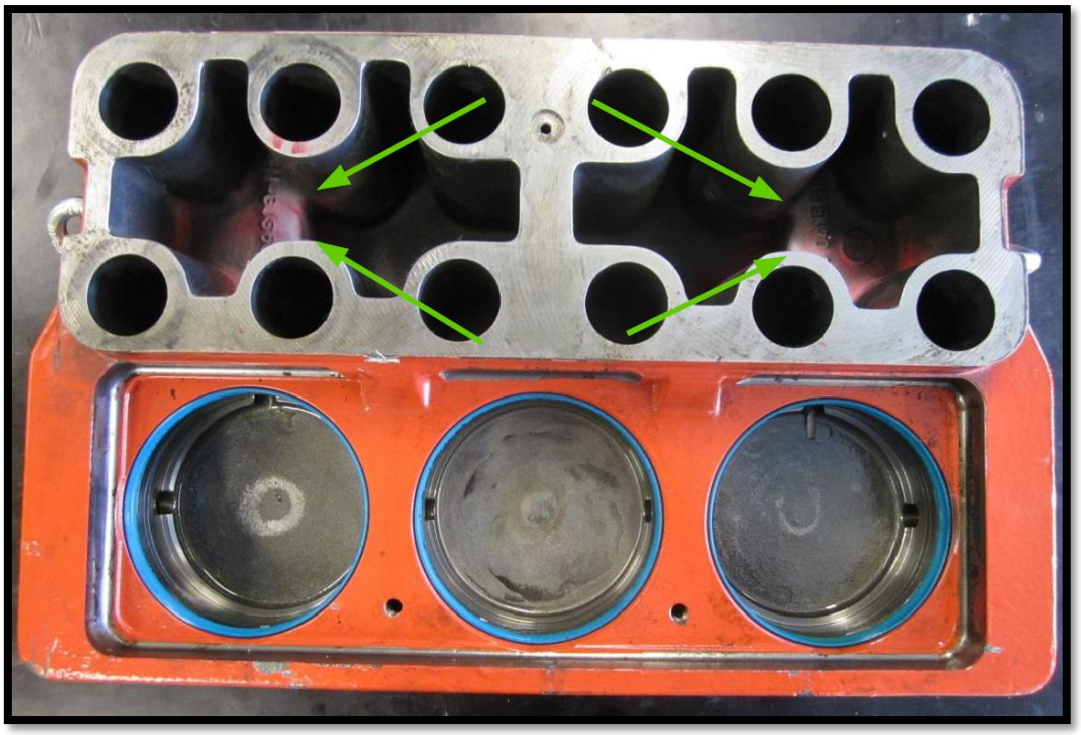

Figure 4: Dye Penetration On Shallowest Section Within The Hollow Section Between Clearance Holes

Figure 5: Suspected Fatigue Cracking Identified Through Dye Penetration

Piston cylinder damage can lead to the undistributed pressure in pistons and therefore will lead to a reduction in efficiency. Over time if this was to worsen then a failure could occur. Typically, form damage of the cylinder is only seen on one of the pistons in a caliper half. This can also lead to unsymmetrical damage of seals leading to their failure which in turn increases Operation and Maintenance (O&M) costs. Figure 6 highlights in yellow the start of damage to the piston cylinder. FEA analysis conducted by Siemens on the structural properties of the component under operational conditions show that the cylinders would experience this type of damage through its lifetime, see Figure 7.

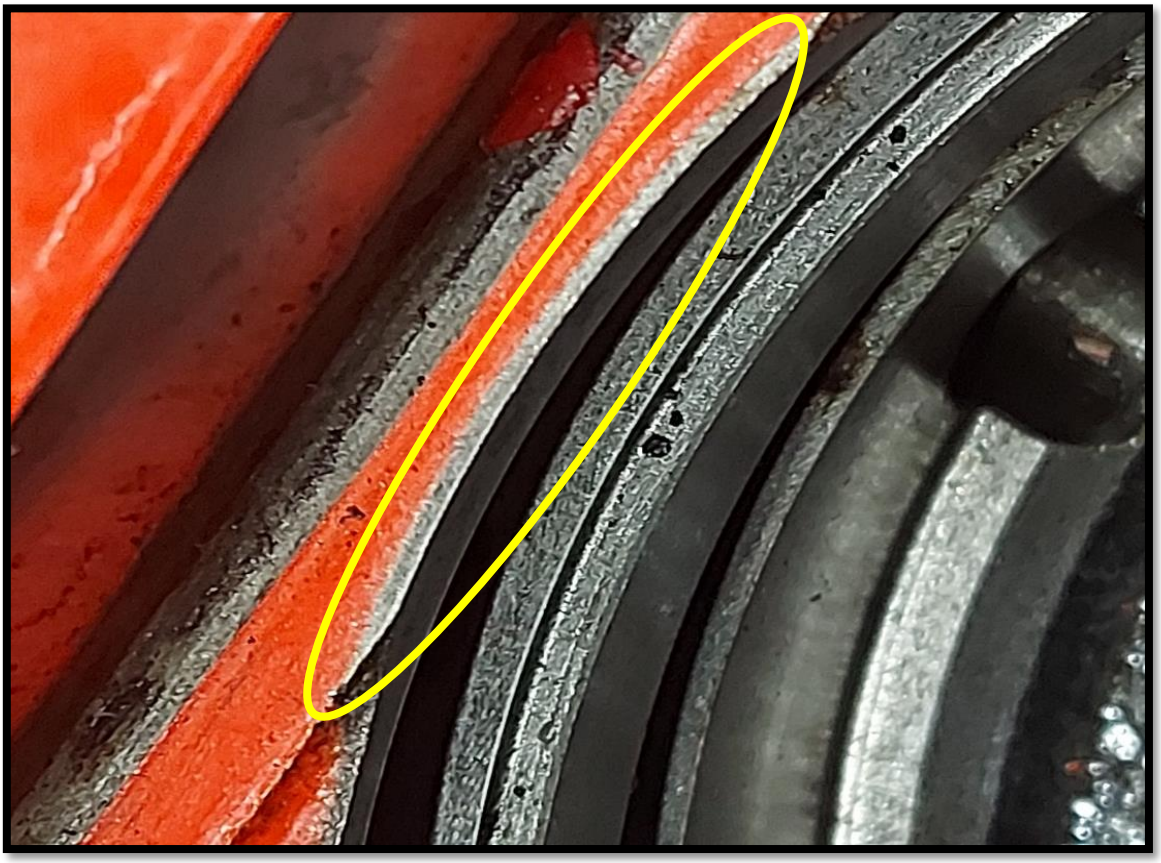

Figure 6: Piston Cylinder Damage

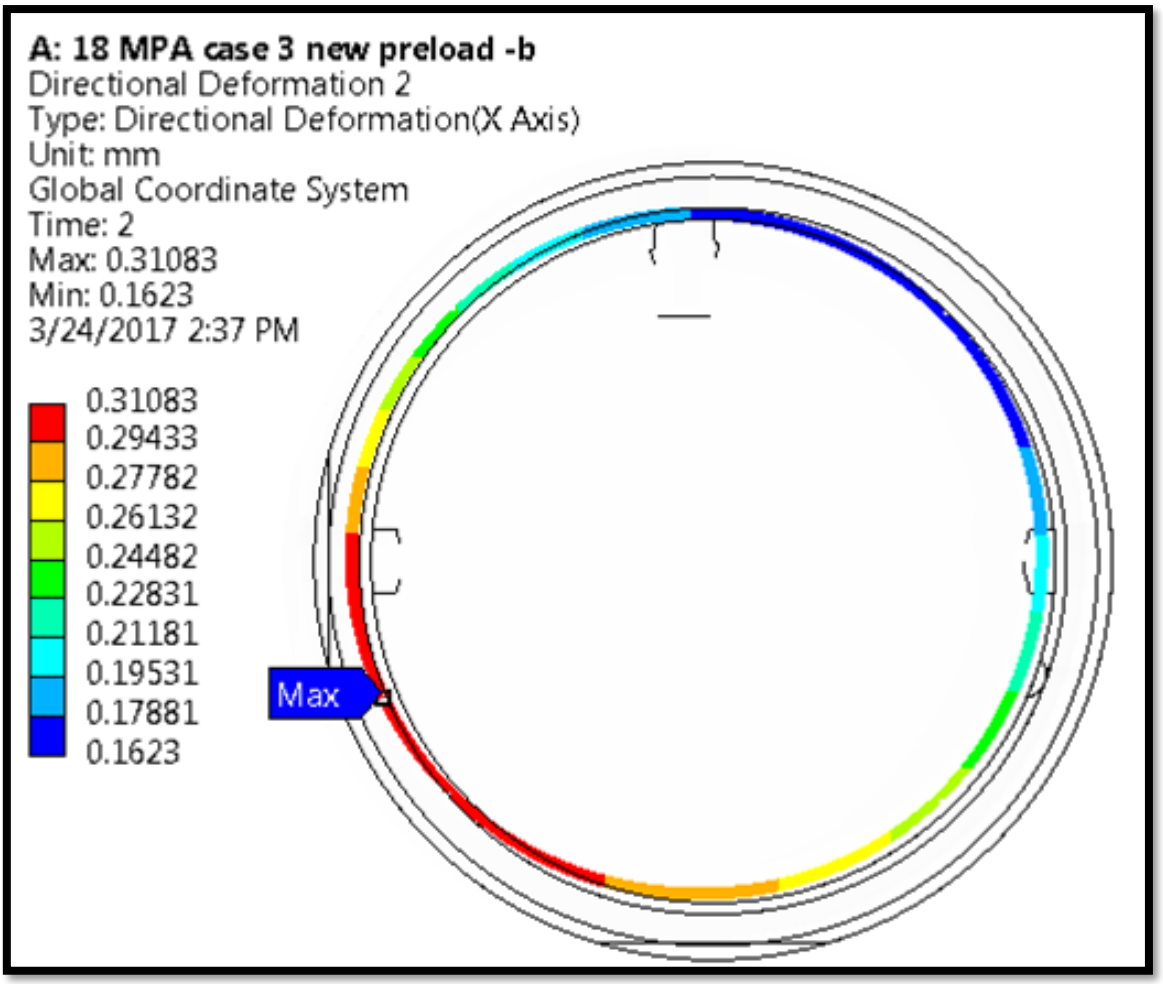

Figure 7: Siemens FEA of Piston Cylinder Deformation [4]

The surface at the bottom of the piston cylinders have shown signs of wearing when compared to new components, see Figure 8. If the surface is being worn down during operation this could lead to oil contamination with metal particles damaging internal components. On the new caliper the bottom on the cylinders have casting defects which appear to have been made by mould movement during casting. Other calipers have shown that grinding has taken place in these areas indicating the removal of these defects. However, these surfaces compared to that in Figure 8 are more rough in nature.

Figure 8: Top - New Caliper with Cast Skin, Cast Defects in Red; Bottom - Used Caliper with Cast Skin Damage

Hydraulic fluid contamination has been apparent from the strip down of the calipers with the fluid showing the oil to be viscous with oil sludge present. This could be from either external or internal sources but overall result in the failure of seals. The operator where Renewable Part Ltd source their components have stated that oil leaks are common and unattended to. This can cause further contamination, reducing the efficiency of the system and leading to higher rates of component wear. Figure 9 showcase the hydraulic fluid contamination observed.

Figure 9: Oil Contamination Seen During Component Strip Down

Brake pads taken from calipers that had been in operation show uneven wear across the brake pad surface, see Figure 10. This is an indication of non-uniformed loading across the surface.

Figure 10: Brake Pad Showing Uneven Wear

2.0 Literature Review

2.1 Common Hydraulic Problems

The concept of hydraulics has been around since 1648 when Blaise Pascal discovered how liquids exert force in all directions when under pressure. This has generated further development in the technology but it was not until 1795 that Joseph Bramah patented the first hydraulic press; this allowed hydraulics to play a key role in the Industrial Revolution [5]. From these many years of practical use in industry hydraulics have become well understood and part of our everyday lives. The common problems with these have also become well understood. Some of the prevailing failures seen by manufactures are [6]:

- Fluid Contamination
- Seal failure
- Mount Connection failure
- Side loading
- Extreme Temperatures
- Over-pressurising

Most of these can be avoided through regular maintenance as per the manufactures instructions as well as being properly designed for the application.

Fluid contamination is the most prevalent and can be caused through leakages or using the wrong fluid for the system. It can lead to pitting on the hydraulic cylinders along with oxidation. Seals can also be deteriorated and fail.

Seal failure can occur for a number of reasons; these include pressure spikes, fluid contamination, high temperatures and incorrect installation. The failure of seals results in the loss of pressure and ultimately reduces system efficiency.

Failure from mounting occurs when the hydraulic components have been misaligned during mounting or have been overloaded. This leads to more wear in certain areas of a component which can lead to failure.

Side loading happens when a hydraulic cylinder applies a force perpendicular to that of the load or direction of movement. This causes the cylinders to experience stain and wear on components that would not be exerted if the hydraulic direction was parallel to that of the direction of movement. Figure 11, shows a diagram of side loading occurring and how it affects the piston and hydraulic system direction.

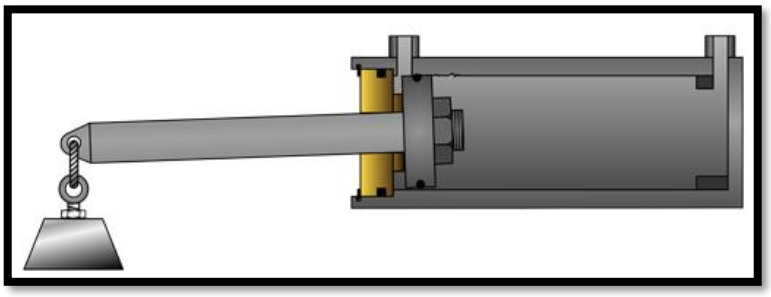

Figure 11: Diagram Showing Side Loading on a Hydraulic Cylinder [7]

Extreme temperatures allow for the material properties of the seals to be altered; with high temperatures causing expansion of the material and cold temperatures making them more brittle. Both conditions can cause seal failure and increase component wear.

Applying pressures greater than that of the recommended operating pressure can cause cylinder and piston deformation or fracture.

An issue that is not as widely known is the poor design of hydraulic systems with regards to fatigue. A failure study carried out by Gianni Nicoletto et al. [8] looked at the failure mechanism of heavy duty hydraulic cylinders. The investigation showed that the cylinder failed due to fatigue that was preventable if fatigue analysis had been conducted. The design of the cylinder had a stress concentration which resulted it its failure. Another failure study carried out by Asad Hameed et al. [9] who investigated cracking on aircraft hydraulic brakes showed a similar story to Gianni Nicoletto et al.'s investigation. Stress concentrations within the design of the part resulted in the initiation and propagation of cracking.

2.2 Wind Turbine Yaw Braking Systems

The first wind turbine to be built was by Professor James Blyth from the University of Strathclyde, formally the Andersonian Institute, when he built a 10m tall turbine to power his holiday cottage [10]. Since then turbine design has evolved considerably with horizontal axis wind turbines being the most common design of commercially available turbines, see Figure 12. While earlier models focused on hydraulic yaw systems, as technology has developed electrical yaw systems are more commonly used [11]. However, a vast amount of turbines still in operation use hydraulic yaw systems.

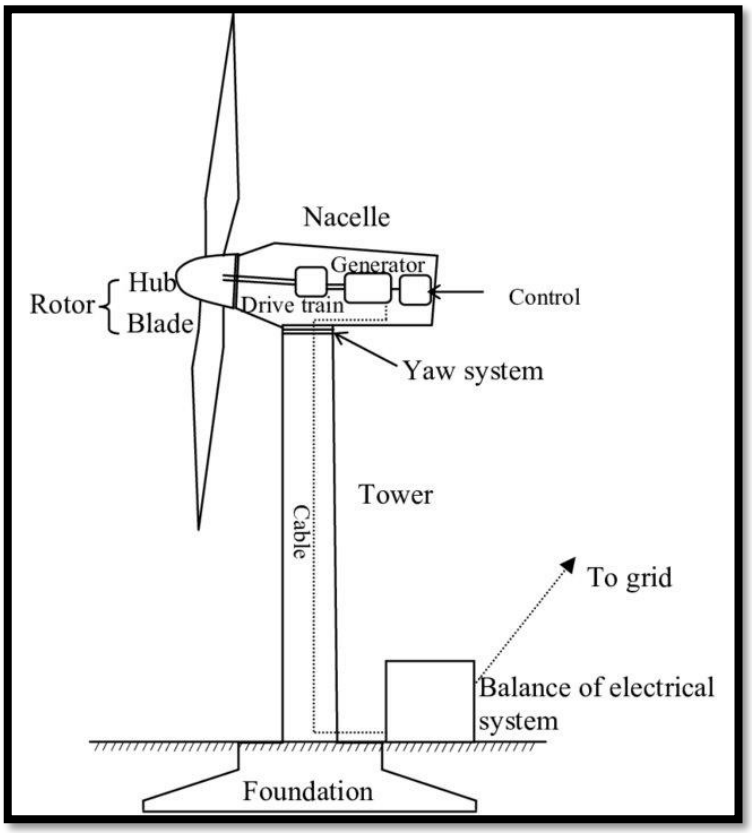

Figure 12: Horizontal Axis Wind Turbine (HAWT) Diagram [12]

The basic function of the yaw system is to turn the rotor into the direction of the wind. This is done through motors that have gears at the end of the drive shaft, see Figure 13. When in operation these move the nacelle around a gear tooth at the top of the tower. The motors will continue to operate until the turbine is facing the desired position at which the braking system will engage. The braking system consists of a set of brake calipers that apply a clamping force to the yaw brake disc. Once stopped the calipers apply a constant clamping force until the nacelle needs to be repositioned, leading to a high number of loading cycles for the calipers.

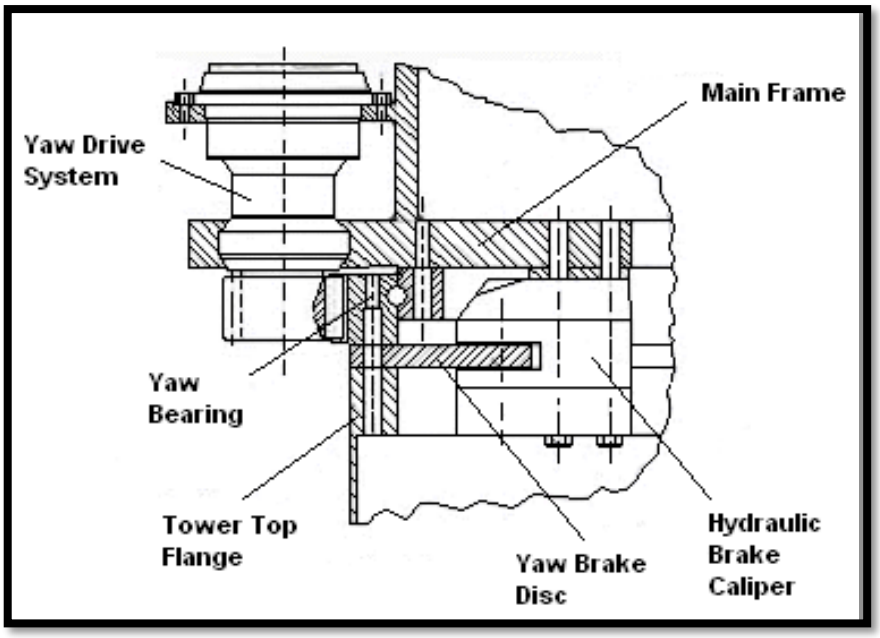

Figure 13: Diagram of Yaw System [13]

2.3 Operation and Maintenance Challenges

2.4 Fatigue

Fatigue is a failure mechanism within materials that causes cracking due to cyclic loading. These loading patterns are often random and therefore hard to predict in design analysis. Fatigue has been analysed in detail since the 1800's but in the last century has been better understood at a microscopic level. Fatigue has two main stages; crack initiation and crack propagation, see Figure 14.

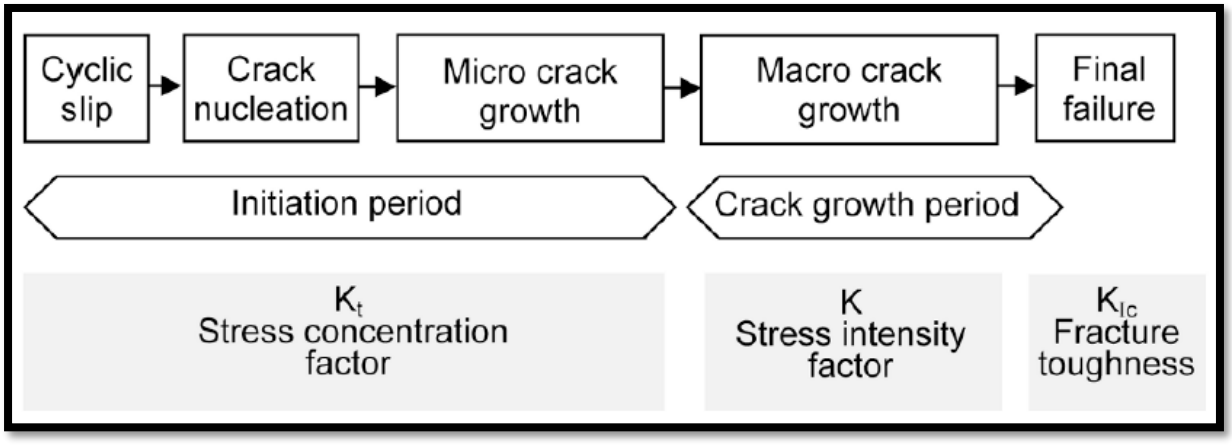

Figure 14: Crack Lifecycle [14]

Within these two stages are sub stages that display the life cycle of a crack. Crack initiation starts after the first cyclic stress has been applied. At this point cyclic slip occurs within the grains at the surface of the material. This is due to grains near the surface having lower stress

levels as a result of the neighbouring environment often being a fluid such as air. This plastic deformation of slip planes causes a monolayer to form out with the surface of the material which will often oxidise. At the same time, strain hardening will occur along the slip band. These two actions make fatigue an irreversible process and in turn make it even more undesirable. Another reason that fatigue occurs at the surface of a material is the inhomogeneous distribution of stresses as a result of surface defects, such as pitting and holes, surface roughness and geometry form.

As cyclic slip continues micro cracks will form, and while these may not always grow, when they do, they begin to join up to different slip systems within the material. The crack will then start to grow past the initial grain boundary but as it reaches more boundaries the rate of cracking is often decreased and in some cases will stop due to structural barriers found within the material. If the crack continues to pass through multiple grains, then both the rate and direction through the following grains are dependent on that of growth through the adjacent grains. This stops the crack rate from being exponential and leads to a crack front forming. This can often be represented as a semi-elliptical shape, see Figure 15. As this crack front moves deeper into the material surface properties no long influence the growth rate and this then become dependent on the resistance within the material [14].

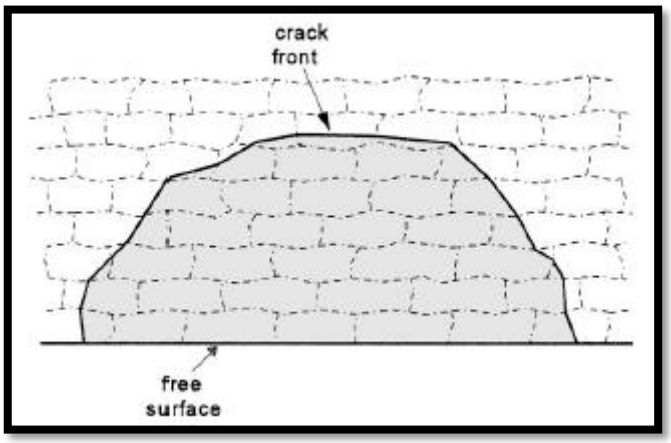

Figure 15: Crack Front Through Grain Boundaries [14]

When designing components, it is difficult to determine the fatigue life and how to design against fatigue. August Wohler developed a method in 1842 in an attempt to predict a material fatigue life after working on a fatigue failure of a train [15]. This led to the creation of S-N curves which are used today in order to give an estimate on the fatigue life of a component. The curves work by comparing maximum stress to failure against number of cycles over a range of cycles, see Figure 16. To obtain these maximum stress values samples are cut from

the material to a standard specimen size and dimension. They are then tested at specific stresses until failure; the corresponding cycles at failure is used to plot the graph.

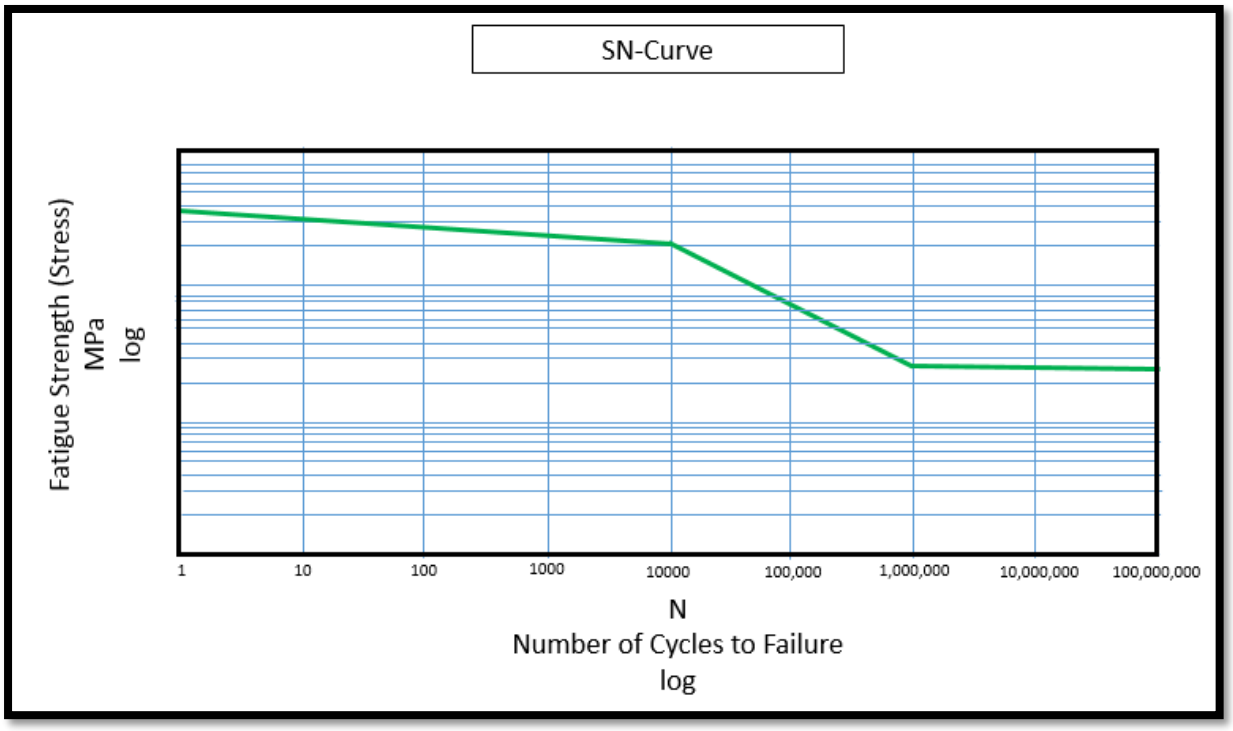

Figure 16: Example of a S-N Curve [15]

There are two areas of fatigue; low cycle and high cycle. Low cycle is when fatigue occurs at a low number of cycles, < 3000 [16]. This type of fatigue is often forgotten about due to systems being designed for high stress cycle applications. However, when looking at systems such as pressure vessels, that only experience loading and unloading a few times a year for inspection, it can then take years to achieve a thousand cycles. This is a reminder that fatigue is a function of cycles and systems are designed to these cyclic lifetimes. High cycle fatigue is the more common area of fatigue and is the more researched of the two. This is when cycles in the range of 10^4 to 10^7 are looked at. At over 10^7 cycles if a material does not show signs of fatigue it is thought that the material will not fail from fatigue; on an S-N curve this will show as a horizontal line called the fatigue limit [16].

When looking at predicting fatigue life it is often difficult to do so without using destructive test methods. This is due to fatigue cracking starting at a microscopic scale. However, if a crack appears during the prorogation stage and can be measured the remaining fatigue life can be calculated from knowing the size of the crack, the material fracture toughness and the loading condition for the crack, see equations below:

$$a_f = \frac{1}{\pi}\left(\frac{K_{IC}}{YS}\right)^2 \quad (1)$$

Where:

a_f – Size of crack at failure

K_{IC} - Fracture toughness of the material

Y – A geometrical factor calculated from the length of the crack in divided by the width of the crack surface (a/W)

S – Stress range for the application

Using this information, the number of cycles to failure based on a crack size on the component can be calculated as per the following:

$$N_f = \frac{2}{C(YS_R)^m \pi^{m/2}(2-m)}\left({a_f}^{1-m/2} - {a_o}^{1-m/2}\right) \quad (2)$$

Where:

N_f - Number of cycles to failure

C – Material constant that is dependent on environment and residual stresses. This can be found in literature

a_f – Crack size at fracture

a_o – Initial crack size at time of inspection

m - Material constant that is dependent on environment and residual stresses. This can be found in literature

Y - A geometrical factor calculated from the length of the crack in divided by the width of the crack surface (a/W)

S_R - Stress range for the application

2.5 Non-Destructive Test Inspection Methods

2.5.1 Dye Penetration Inspection

When fatigue cracking is suspected on a part often Dye Penetration tests are conducted to identify the presence of cracks. This works by applying a low surface tension fluid to a surface. If cracking is present; the fluid, known as a penetrant, flows into the crack. The excess penetrant is then cleaned from the surface leaving some behind in the crack. A developed is used to draw out the penetrant from the crack, making it visible to the inspector. There are two type of penetrant fluorescent or non-fluorescent with fluorescent requiring an ultra-violet light. This method has been used since the 19th century but relies heavily on the surface being completing clean which is often hard for rough surfaces. As a result, rough surfaces such as cast iron commonly show false positives [17].

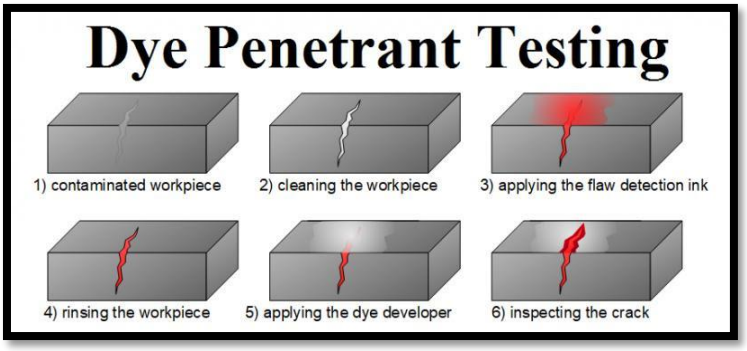

Figure 17: Dye Penetrant Testing Method [18]

2.5.2 Ultrasonic Testing (UT)

Ultrasonic testing is carried out by placing a transducer onto a part where high frequency waves are propagated through it. Within the transducer a piezoelectric element is excited via electrical energy which in turn causes the atoms in the element to oscillate producing the high frequency sound waves. These waves move through the material and are reflected back to the transducer once a boundary is met. When no defects are present this boundary is the oppose side of the part that is open to the air or another medium. When a defect is found in the part the sound waves are reflected back from it giving a different amplitude to that found elsewhere in the part, see Figure 18. These wave amplitudes are recorded and used to produce an image of the affected area with defect measurements. As these boundaries are required to carry out UT a medium, such as a gel or water, is used on the surface so that air cannot give false readings. Rough surfaces, like those seen in cast iron, can cause problems and therefore immersion testing occurs. This is when the part is immersed in water so that accurate result can be obtained [19].

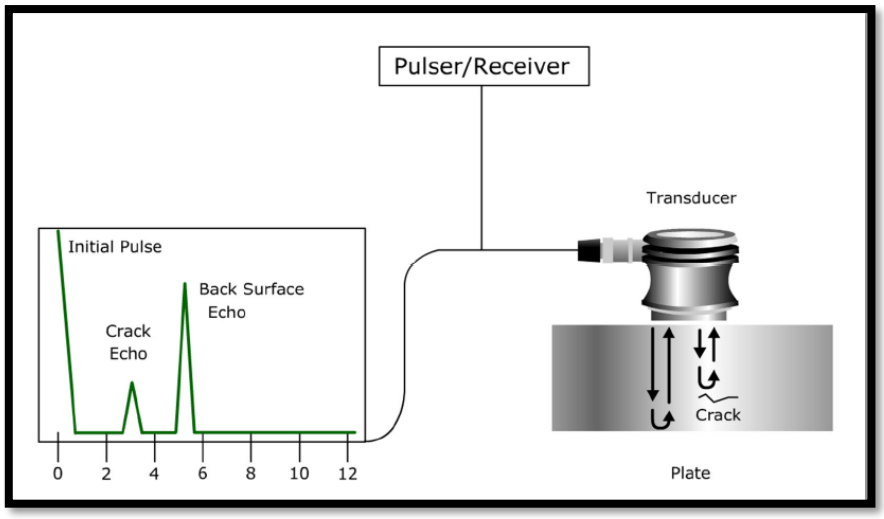

Figure 18: Ultrasonic Testing Method Diagram [19]

2.5.3 Eddy Current Testing

Eddy current testing operates by creating a magnetic flux from passing an alternating current through a solenoid. These magnetic fields are presented to a conductive material via a probe that houses the solenoid. This creates eddy currents within the material which form circular paths in the opposite direction to that of the current within the solenoid. These eddy currents produce their own magnetic flux which opposes that of the magnetic flux in the solenoid. Defects in a material interrupt the pathway of the eddy currents lowering the magnetic flux from them, see Figure 19. This can be measured and used to produce an image of the affected area with defect measurements. This method is good for identifying surface cracks and surface roughness quickly without the need for surface preparation [20].

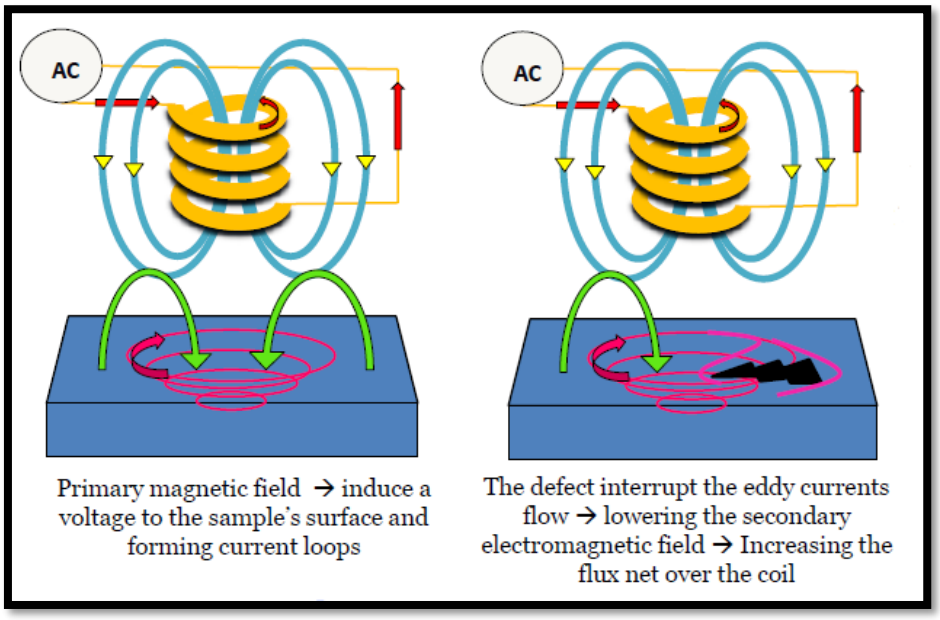

Figure 19: How Defects are Identified in Eddy Current Testing [20]

2.5.4 Radiographic Testing

Radiographic testing, commonly known as X-Ray testing, can be used to detect defects within a material. This is done by emitting radiation onto a part where a radiographic film is present on the opposite side, see Figure 20 . Different levels of radiation received on the film result in a black and white image of the parts bulk material. This is a costly and time consuming process but is very reliable [21].

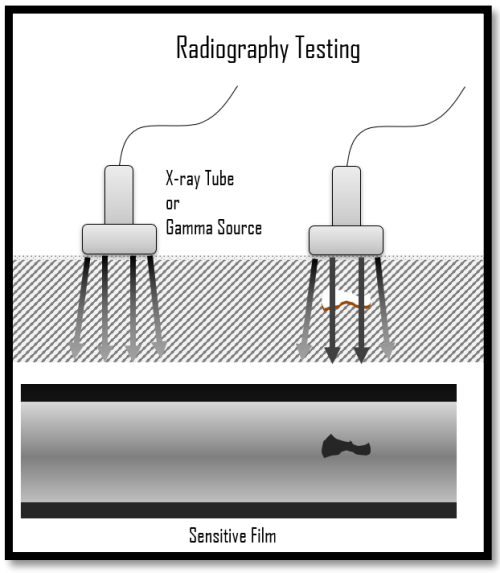

Figure 20: Example of Radiography Testing [21]

2.6 Cast Iron

Cast iron has many benefits compared to other materials such as low cost, excellent machinability and has good vibration damping properties. These make cast irons suitable for braking systems when compared to other materials. However, due to the high carbon content, which gives them vibration damping characteristics, fatigue life is lower and increases the materials proneness to fracture. There are a variety of different cast irons which each have a different matrix of carbon in the form of graphite. Some of the most common commercially available cast irons include grey, and ductile cast iron. Grey iron has graphite formed in flake like shapes whereas ductile cast iron has graphite in spherical form. This affects the internal microstructural of the material with grey iron being more susceptible to fatigue cracking but are more notch resistant compared to nodular cast irons [22]. The effect these properties have can be seen in Figure 21 where nodular is clearly more fatigue resistant. The flaking form of graphite causes stress concentrations at the tips of the flakes which allow for crack initiation and propagation to occur more easily.

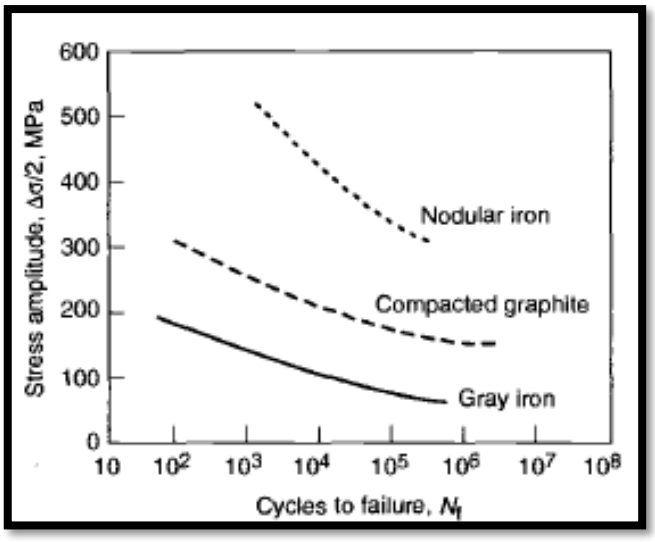

Figure 21: S-N Curves Comparing Different Cast Iron Types [22]

When looking at fatigue design of components FEA analysis and probability models can be used to estimate life under certain loading conditions [23]. These models rely on experimental data to create S-N curves that allow for calculations to be completed. As fatigue is a result of surface defects, fatigue experiment are carried out by creating a machined specimen such as seen in Figure 22, a notch is placed on the surface to simulate a defect and the specimen undergoes cyclic loading.

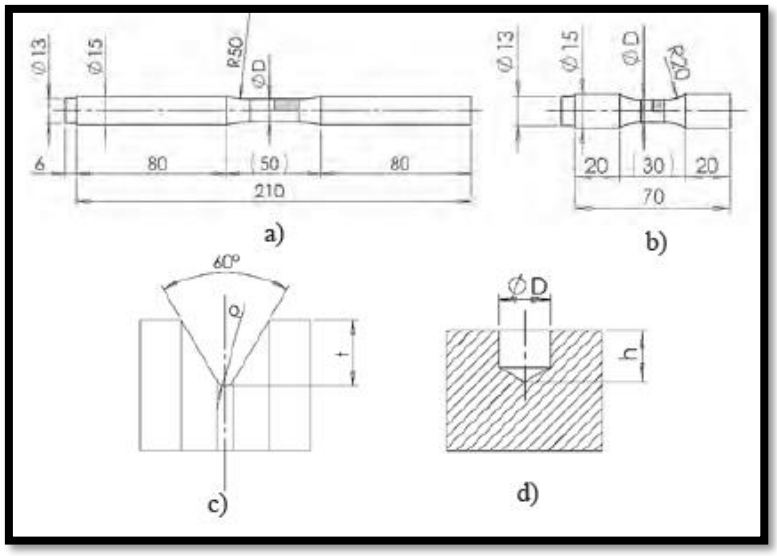

Figure 22: Fatigue Testing Specimen Design - a.) rotating bending specimen, b.) tension compression specimen, c.) circumferential notch geometry, d.) drilled hole geometry. [23]

This has been proven as an effective way to show fatigue within a structure but when looking at cast components one important aspect is often over looked. A casting skin is formed, see Figure 23, from the sand cast process due to a range of variables; including cooling rate, sand

quality and binder. This is called decarburisation and is when moisture in the mould and atmosphere interact with each other causing a layer of reduced graphite [24].

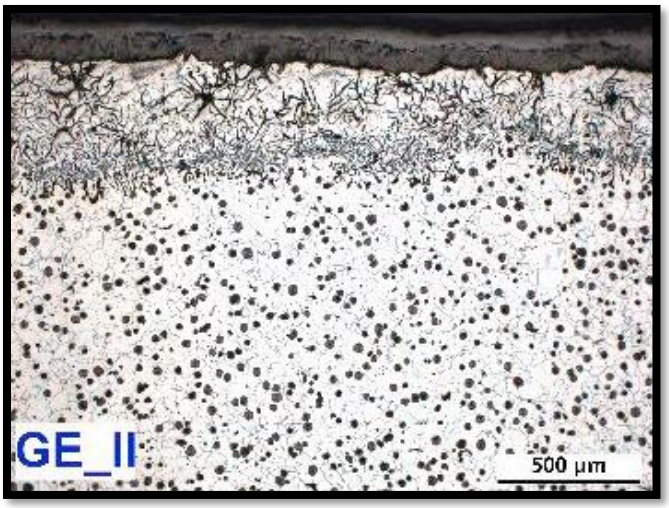

Figure 23: EN-GJS-400-15 With Rim Of Lamellar Graphite In Pearlite Matrix With Surface Roughness [25]

A study carried out by Kim Bergner et al. looked at the fatigue properties of EN-GJS-400-15 with and without a casting skin. These experiments took place in the form of dog bone fatigue tests looking at surface roughness only. It was found that specimens with a rough surface saw a fatigue strength reduction of 18% and those with a surface roughness and casting skin saw a 34% reduction [26].

3.0 Technical Analysis

3.1 Calipers Environment

The calipers that Renewable Parts Ltd source come from offshore farms, three of these locations were given and the temperature difference analysed. This was done to see if any thermal fatigue could be taking place over a components service life. Figure 24 shows the maximum and minimum temperatures experienced at the three sites over a year. These values come from historical weather data at a distance of 2m above sea level [27]. The calipers, which are housed in the nacelle, were located ~80m above sea level. This means that the temperature are likely to be different than that seen in Figure 24 but it does show an indication to the temperature ranges that would be experienced. As the range is between 0 - 25°C it was determined that for cast iron material no effect would be experienced. However, the seals within the part may face some signs of fatigue and should be investigated further in the next phase of the project.

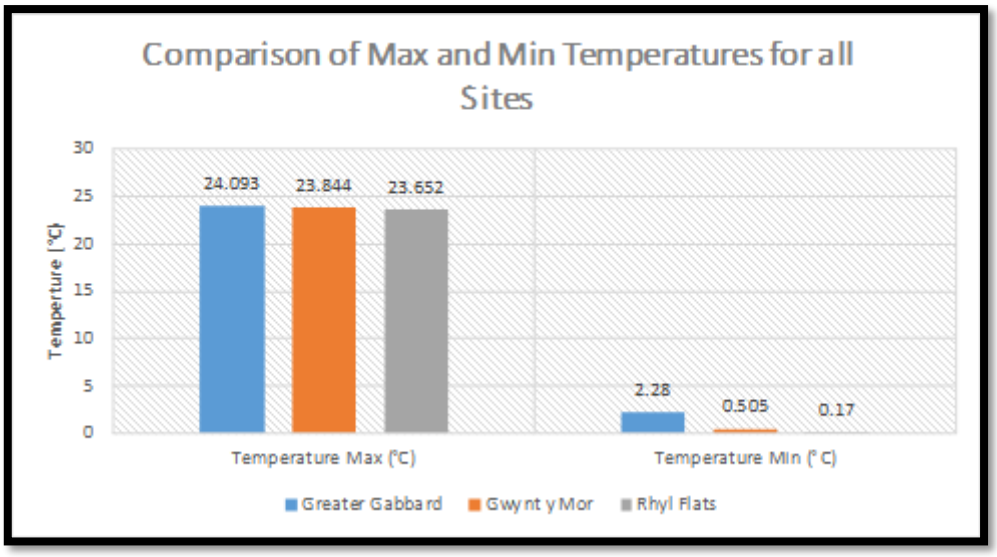

Figure 24: Comparison of Maximum and Minimum Temperatures at the Three Sites

3.2 Breaking Force

Svendborg's datasheet for the calipers provides three equations to work out the forces applied from operations. These include braking torque (M_B), braking force (F_B) and clamping force (F_C):

$$M_B = a \,.\, F_B . \frac{D_B}{2} \; [Nm] \tag{3}$$

$$D_B = D_O - 0.136 \; [m] \tag{4}$$

$$F_B = F_C \,.\, 2 \,.\, \mu \; [N] \tag{5}$$

$$F_C = A \,.\, P \,.\, 10 \; [N] \tag{6}$$

Using these set of equations the forces exerted by the calipers were calculated using the information from Table 2. This resulted in an overall braking torque of 7.9MNm for the turbine as well as a braking force of 0.835MN and a clamping force of 1.04 MN per caliper. This means that each caliper half applies a braking force of 417.6 kN and a clamping force of 522 kN. Applying Newton's Third law, which states that:

"*Whenever one object exerts a force on another object, the second object exerts an equal and opposite on the first.*" [28]

This means that the clamping force applied by the caliper will result in a normal force of equal value being applied to the yoke of the caliper half.

Table 2: Braking Equations Variables

Braking Equations Variables			
Variable	Notation	Value	Reference
Braking Torque (Nm)	M_B	7,897,651.20	N/A
Braking Force (N)	F_B	835,200.00	N/A
Effective Braking Diameter (m)	D_B	2.364	N/A
Outer Disc Diameter (m)	D_O	2.5	[4]
Clamping Force (N)	F_C	1,044,000.00	N/A
Brake Pad Area (cm^2)	A	580	[29]
Pressure of Calipers (Bar)	P	180	[29]
Friction Coefficient	μ	0.4	[29]
Number of Brakes	a	8	[4]

3.3 CAD Modelling

It was determined that in order to create a fatigue test fixture and conduct FEA for validation of this, a CAD model would be required. This has been created from a mixture of caliper drawings (see Appendices) and measurements from a new component. No geometrical tolerance data was able to be sourced for the part. The mounting holes, piston cylinders and overall dimensions are accurate as per the manufactures specification. Other features on the part have been measured and therefore due to unknown manufacturing tolerances these may not be the specified nominal sizes. Other form dimensions have been calculated from measuring the drawing and using the drawing scale. However, the overall form has been deemed sufficient for the modelling of a test fixture and initial FEA modelling to estimate the testing effects and potential fatigue areas. Figure 25, Figure 26 and Figure 27 show the model with painted surfaces in red, machined surface in polished steel and cast skin surfaces in cast iron grey.

Figure 25: Isometric Views of CAD Model of BSAB-S-120

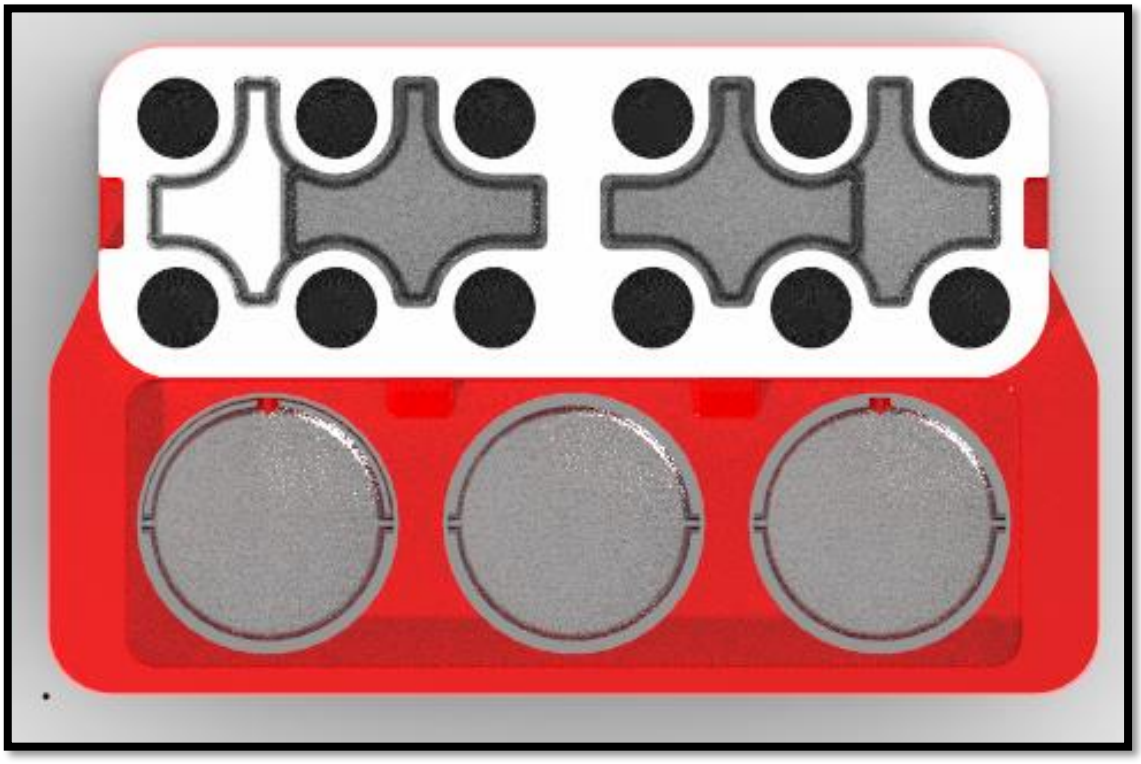

Figure 26:Top View of CAD Model of BSAB-S-120

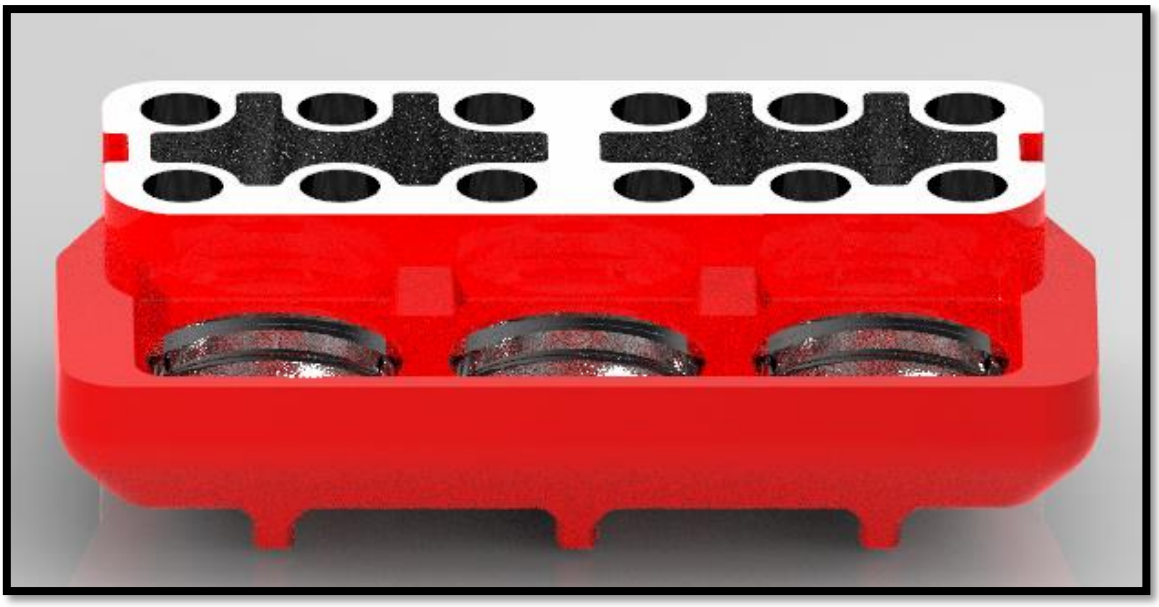

Figure 27: Front Isometric View of CAD Model of BSAB-S-120

3.4 Fatigue FEA on Caliper

Finite Element Analysis (FEA) was carried out on the caliper half to identify any areas of potential fatigue. Ansys 17.2 was used to carry out the analysis. Material property data for EN-GJS-600-3 was sourced from BS ISO 1083:2018, see Appendix 4. S-N curve data was sourced from literature where fatigue testing on EN-GJD-600-3 has produced a S-N curve with an equation[17]; this equation was used to calculate different alternating stresses, see Figure 28. Data from Phase 1 of the project was used to analyse the Ultimate Tensile Strength, Poisson's ratio and yield strength being calculated from tensile tests, see Table 3 and Appendix 5.

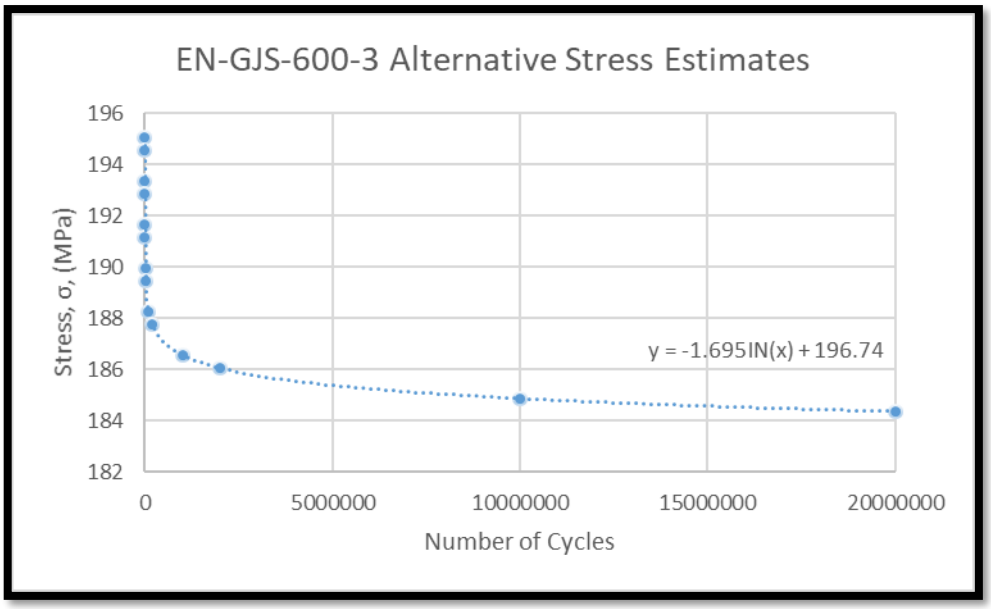

Figure 28: EN-GJS-600-3 Alternative Stress Estimates [30]

Table 3: Material Properties Calculated from Project Phase 1 Tensile Strength Test

	Material Property	Test 1	Test 2	Test 3	Test 4	Average
Caliper 31	Poisson Ratio	0.65915	0.221332	0.325438	-	0.40
	Yield @ 0.2% Calculated (MPa)	277.4476	216.6215	243.4596	-	245.84
	UTS (MPa)	560.88	538.67	551.73	-	550.43
Caliper 4	Poisson Ratio	-	0.429355	0.220019	0.26548	0.32
	Yield @ 0.2% Calculated (MPa)	-	285.98	231.49	257.73	258.74
	UTS (MPa)	-	609.61	602.5	597.59	606.06
Total Averages	**Average Poisson Ratio**	**0.36**				
	Average Yield Stress @ 0.2% (MPa)	**252.29**				
	Average UTS (MPa)	**578.24**				

3.4.1 Geometry and Meshing

No geometry simplification was carried out for the part to ensure results gave an accurate representation of the effects on the geometry for the part under the loading conditions. A tetrahedron mesh with a 5mm element sizing was applied, see Figure 29. This meshing was used to analysis the caliper without any defects.

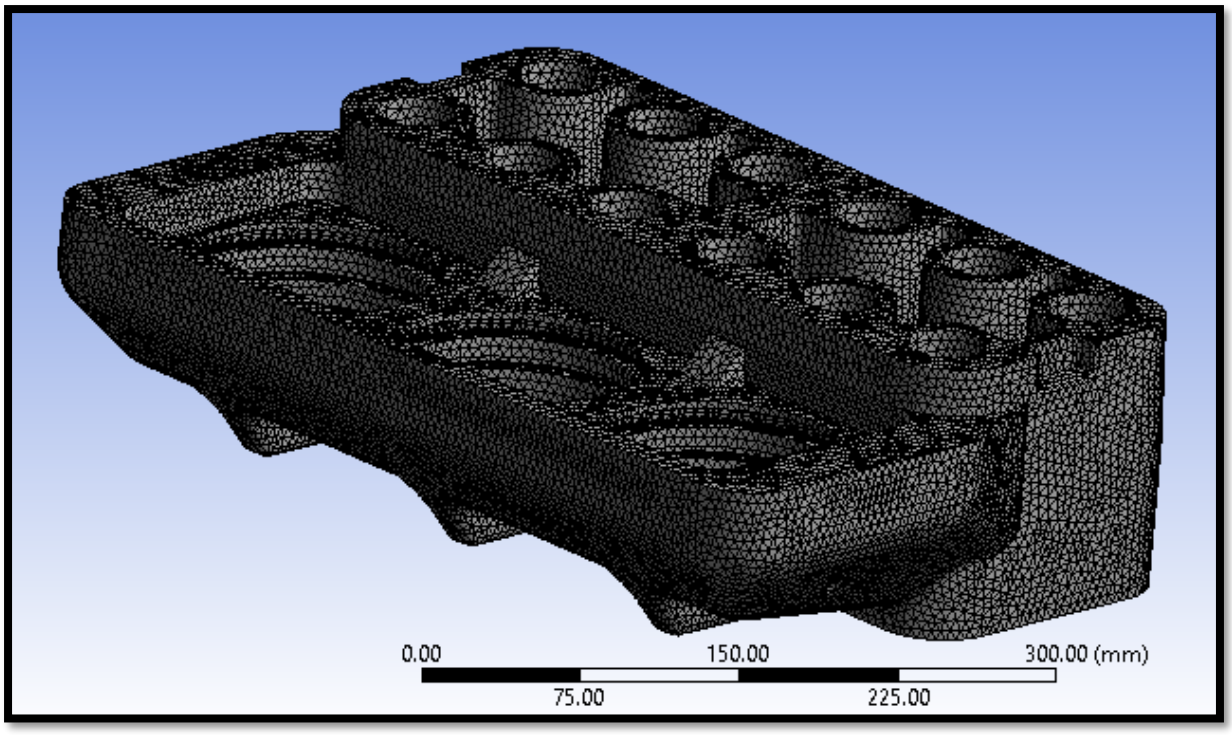

Figure 29: BSAB-S-120 FEA Meshing

Fracture cracks were added to four models to demonstrate the effects of cracking on the ledge surface within the cavity between the mounting holes. All cracks were located on a coordinate system offset from the global coordinate system at X:106, Y: 58.8 and Z: -247. This location was chosen as it represents the rough location of the defect found in Figure 5. The fracture geometry used for the crack was a semi-elliptical crack with a minor radius of 1mm and a major of 3mm. Meshing method for the cracking was hex dominant with three meshing contours around the crack front, see Figure 30.

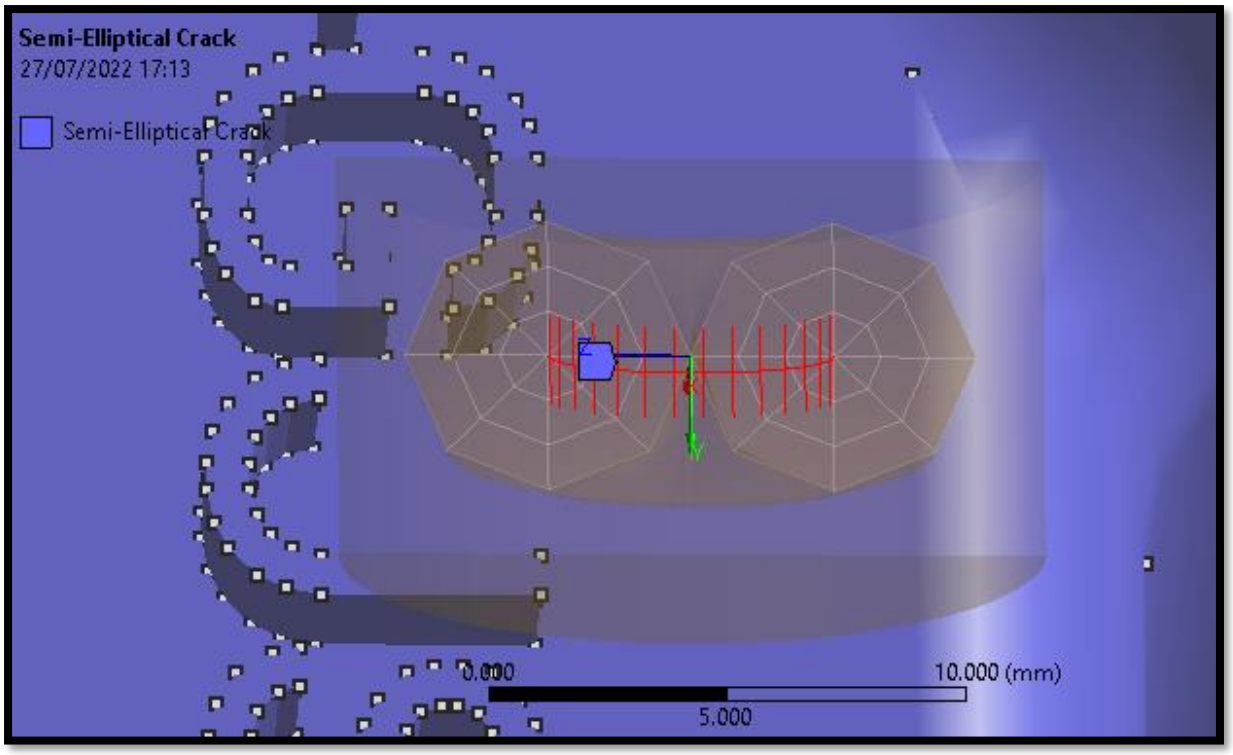

Figure 30: Fracture Geometry and Meshing

3.4.2 Loading Setup

All models used the static structural mode within Ansys. Every model was setup with the bottom mounting face set as a fixed support. For the loading conditions maximums were used to evaluate worst case scenarios. The clamping force, calculated to be 522kN, and the braking force, calculated to be 987kN, were used. However, there were two loading positions for these forces. Loading 1 applied the normal clamping force to the bores and the breaking force, as a moment, to the surface at the top of the bores, see Figure 32. Loading 2 was placed on the corner of the caliper to simulate the maximum deformation seen in Figure 31, as this showcases the combination of both normal and tangential forces in a lab environment, see Figure 33. This represents the actual loading conditions more and shows how the caliper is effected from real

world scenarios. Fatigue was modelled as zero based meaning that the forces are applied and returned to the zero position.

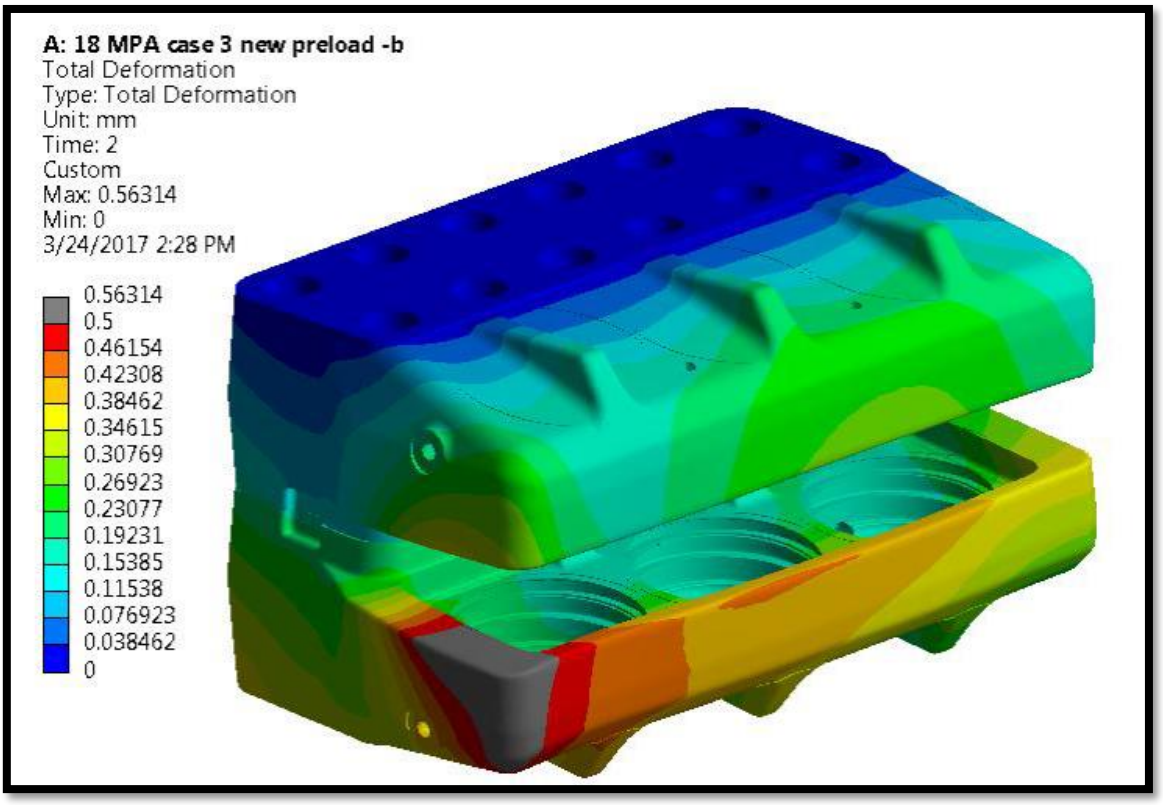

Figure 31: FEA Deformation Analysis Results from Siemens Structural Investigation [4]

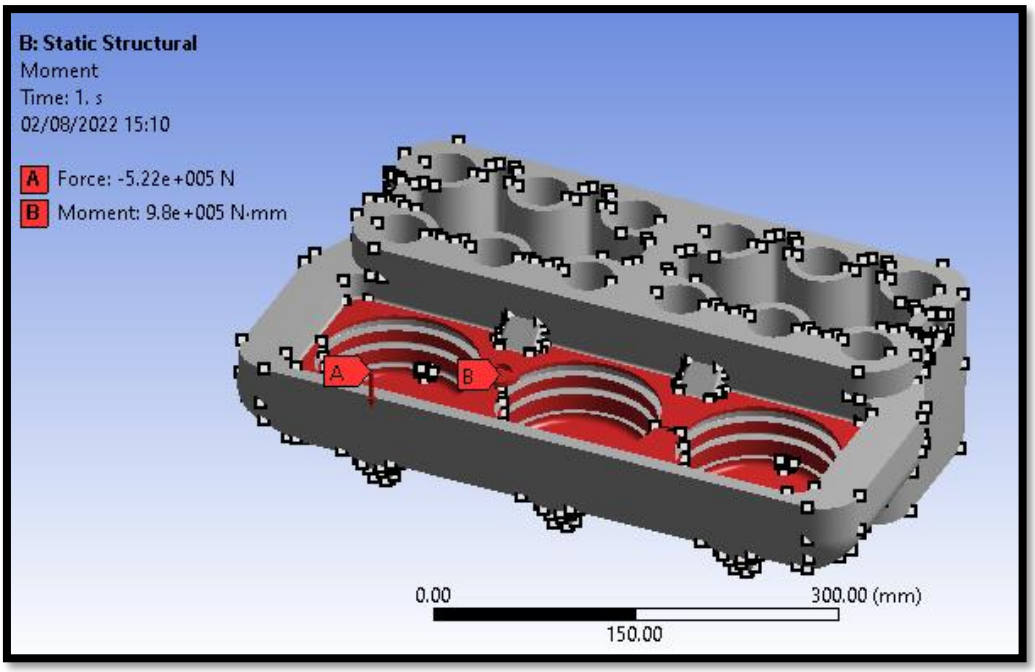

Figure 32: Loading 1 Setup

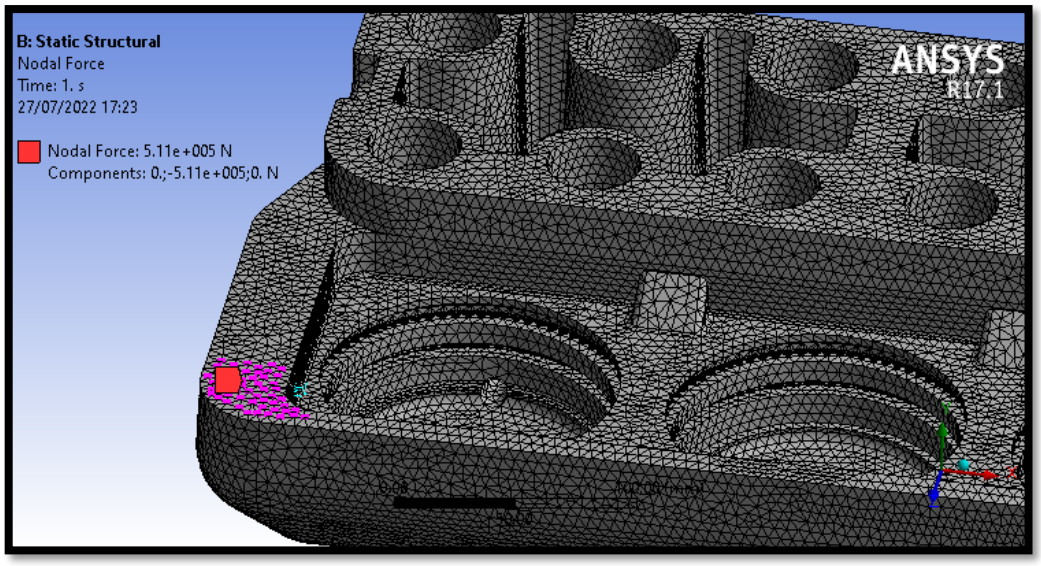

Figure 33: Loading 2 Setup

3.4.3 FEA Results

From Loading 1 there was no evidence of fatigue within the cavity at the holes. This area had the lowest deformation for the whole part, see Figure 34. A stress concentration was noted at the corner near the stamping, see Figure 35, which is at the same location as the suspected crack in Figure 5. Even with this stress concentration no fatigue damage appeared in this area. This would indicate that the component is unlikely to fail at this location. For this loading condition failure was estimated to occur on the underneath of the part at the supporting fins, see Figure 36.

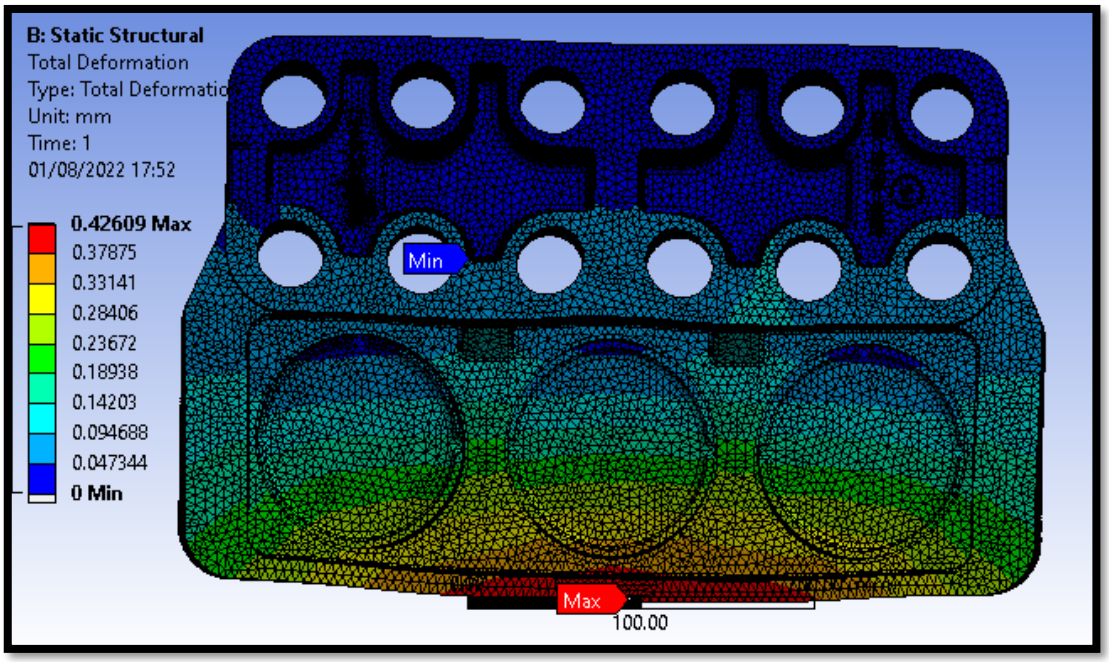

Figure 34: Stamped Caliper Model with Loading 1 - Deformation Result

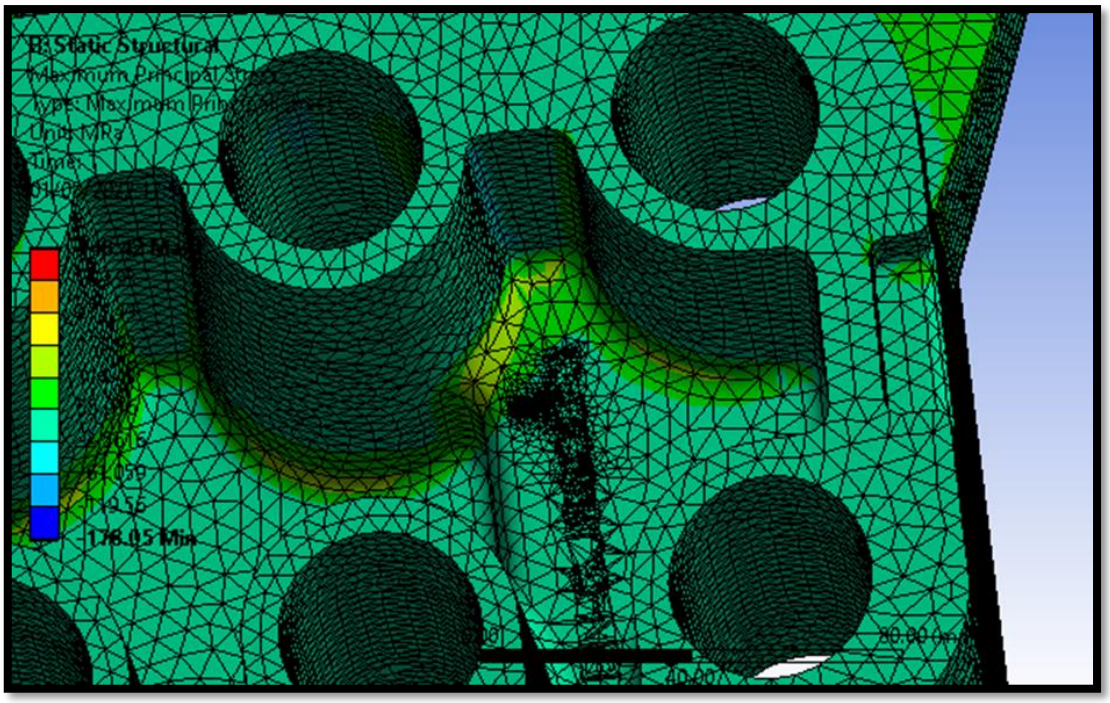

Figure 35: Stamped Caliper Model with Loading 1 - Stress Concentration on Cavity Ledge Corner

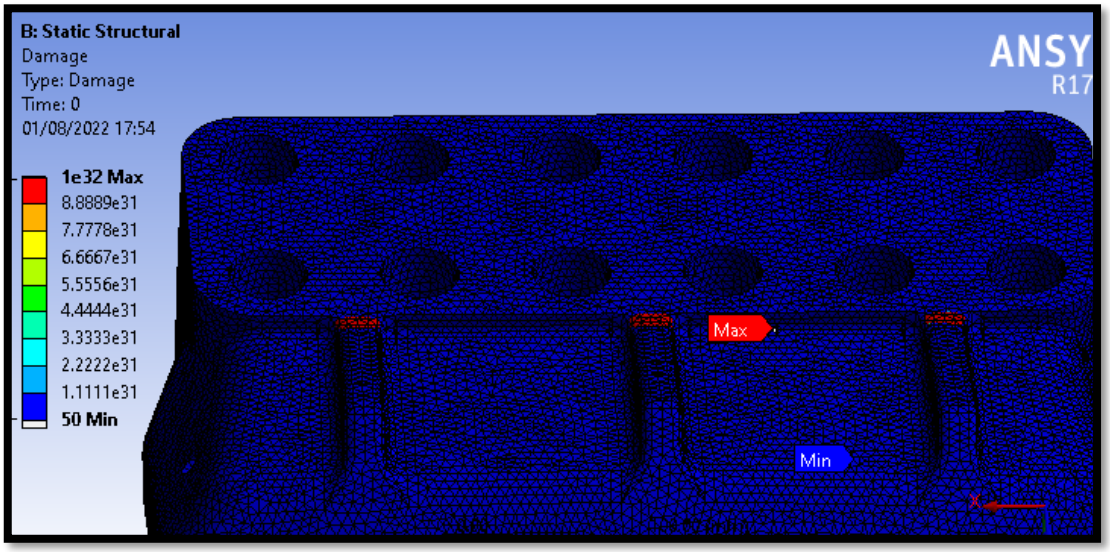

Figure 36: Stamped Caliper Model with Loading 1 - Damage Location from Fatigue

Loading 2 showed a similar story to that of loading 1 in terms of deformation with the ledge surface experiencing the lowest values, see Figure 37. A stress concentration of bigger magnitude was seen in the corner near the stamping, see Figure 38. When looking at fatigue damage Loading 2 resulted in damage being seen on the ledge surface, see Figure 39. However, this was not the only damage area with areas underneath the bores likely to fail first under these loading conditions, see Figure 40. This shows that an undistributed loading would cause failure at the cavity location but under the conditions as per Loading 1 this would not be the case. As

fatigue failure occurs at stresses lower than that of the materials strength by applying a low load at the position seen in Loading 2 may cause the component to fail as per reported by Renewable Parts Ltd.

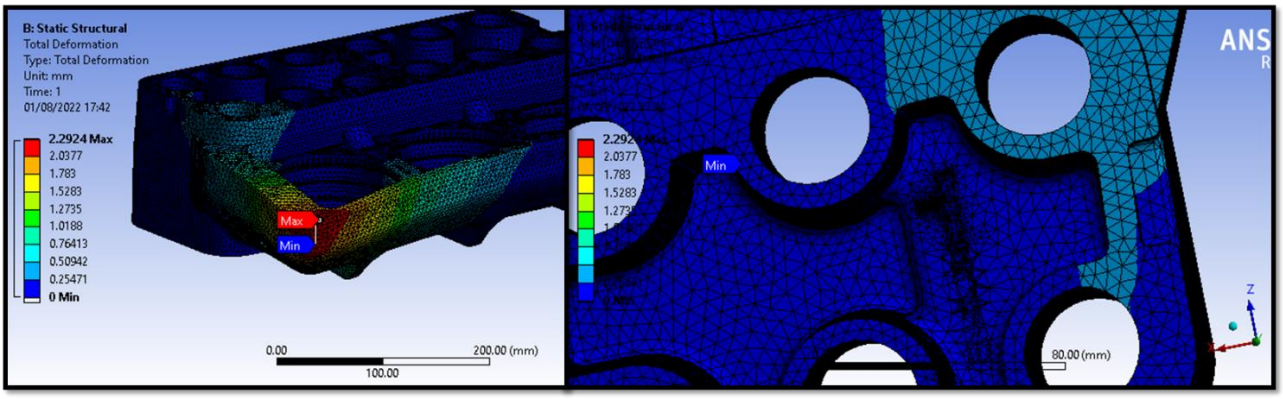

Figure 37: Stamped Caliper Model Loading 2 - Deformation Result

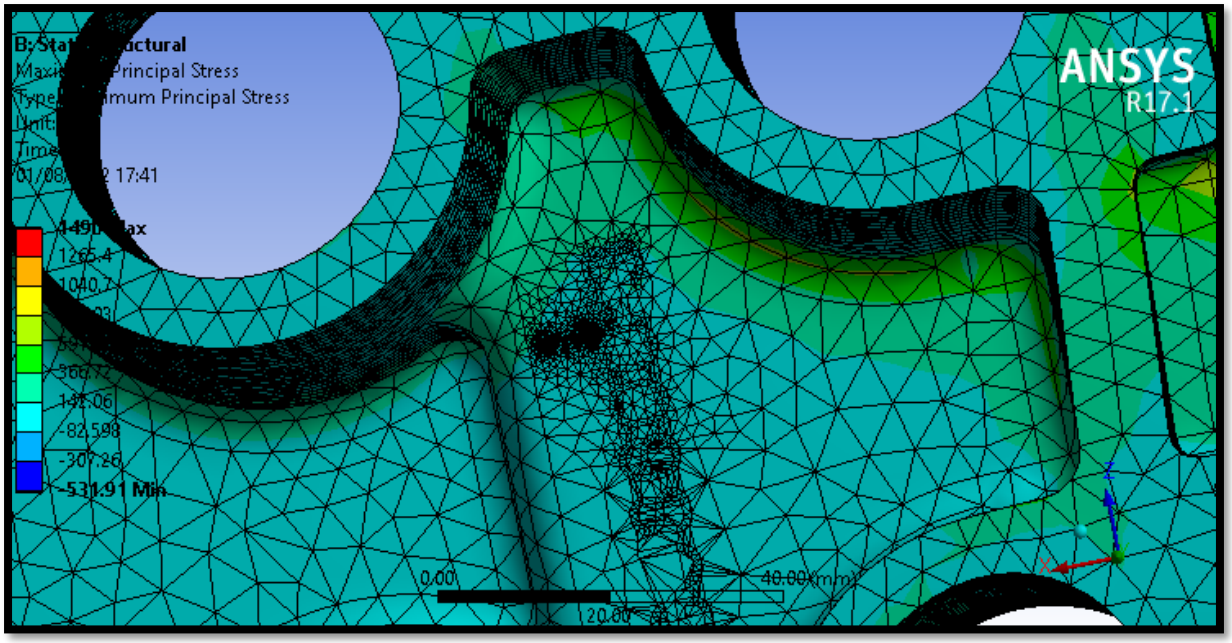

Figure 38: Stamped Caliper Model Loading 2 - Stress Concentration on Ledge Surface

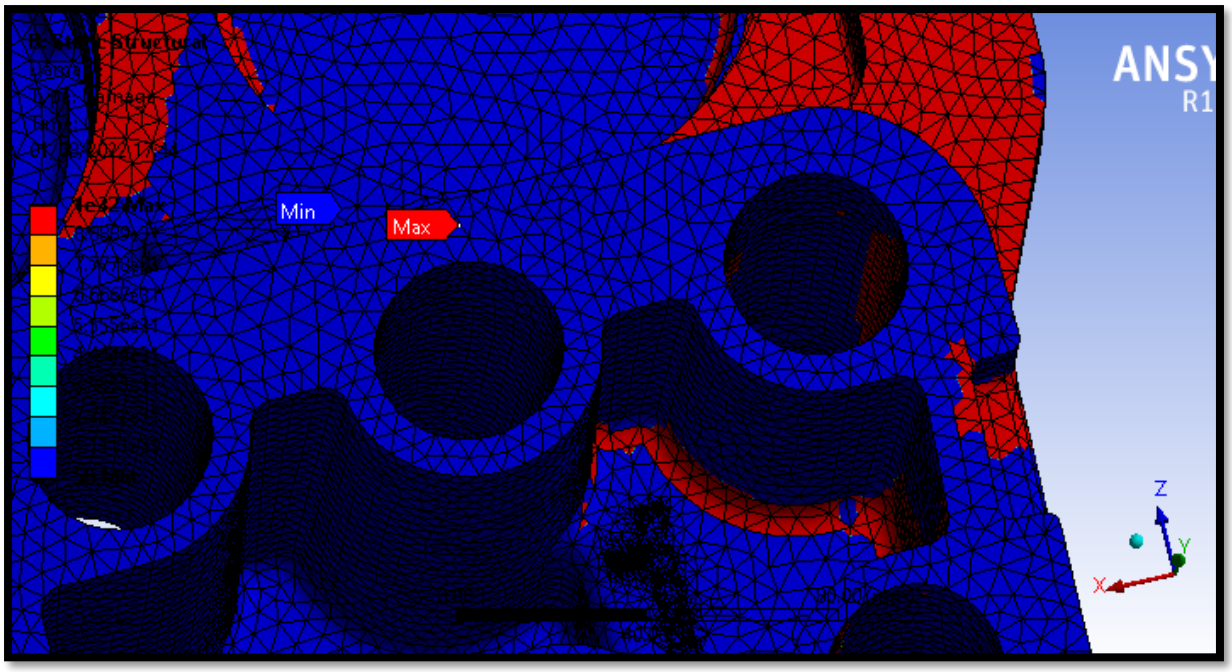

Figure 39: Stamped Caliper Model Loading 2 - Fatigue Damage on Ledge Surface

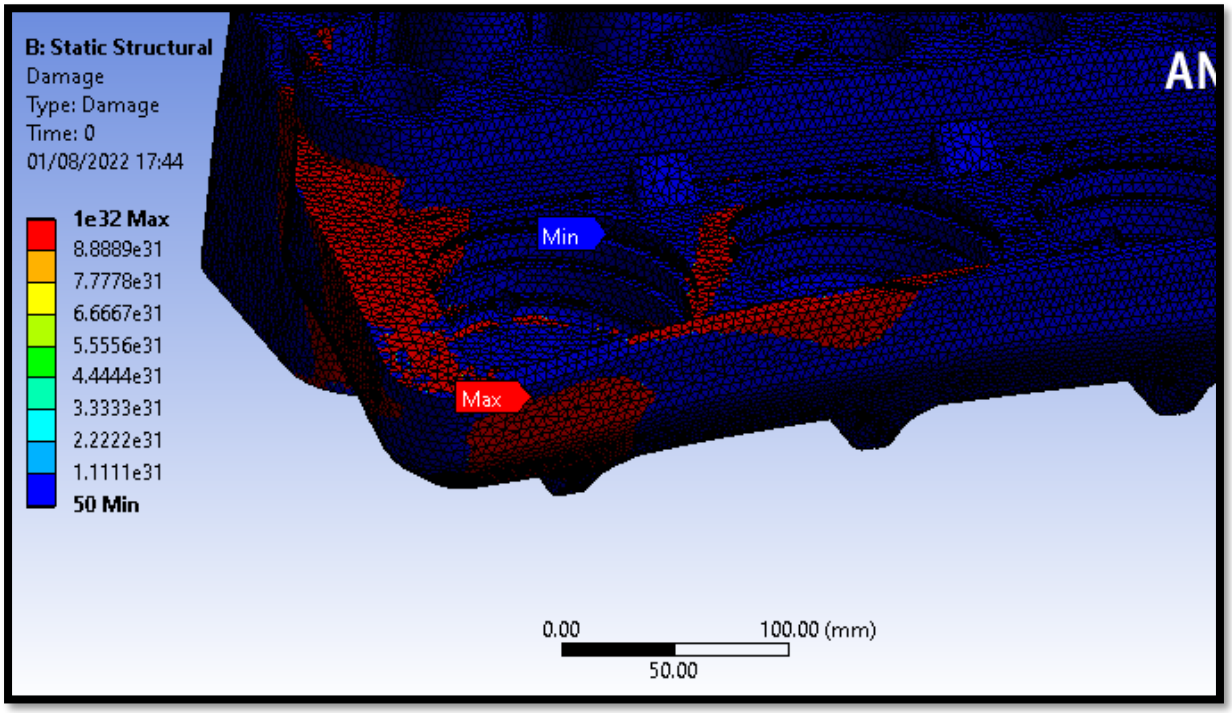

Figure 40: Stamped Caliper Model Loading 2 - Fatigue Damage of Full Component

3.5 Metallography Analysis of Cast Material

Metallography analysis was carried out of identify any flaws within the material that may of arisen from either during or post manufacture. From this it was hoped that a better understanding of how the component was reportedly experiencing fatigue cracking would be gained. As well as this identifying the effects from removing cast defects from the bores was also of interest.

3.5.1 Sample Creation

Material was extracted from an out of service caliper at locations A and B, see Figure 41. Sample A was taken to analysis the effect from grinding cast surface defects within the bores to see if this has changed the material properties at this area. Sample B was taken to analysis the cast surface and see if any fatigue cracking was forming.

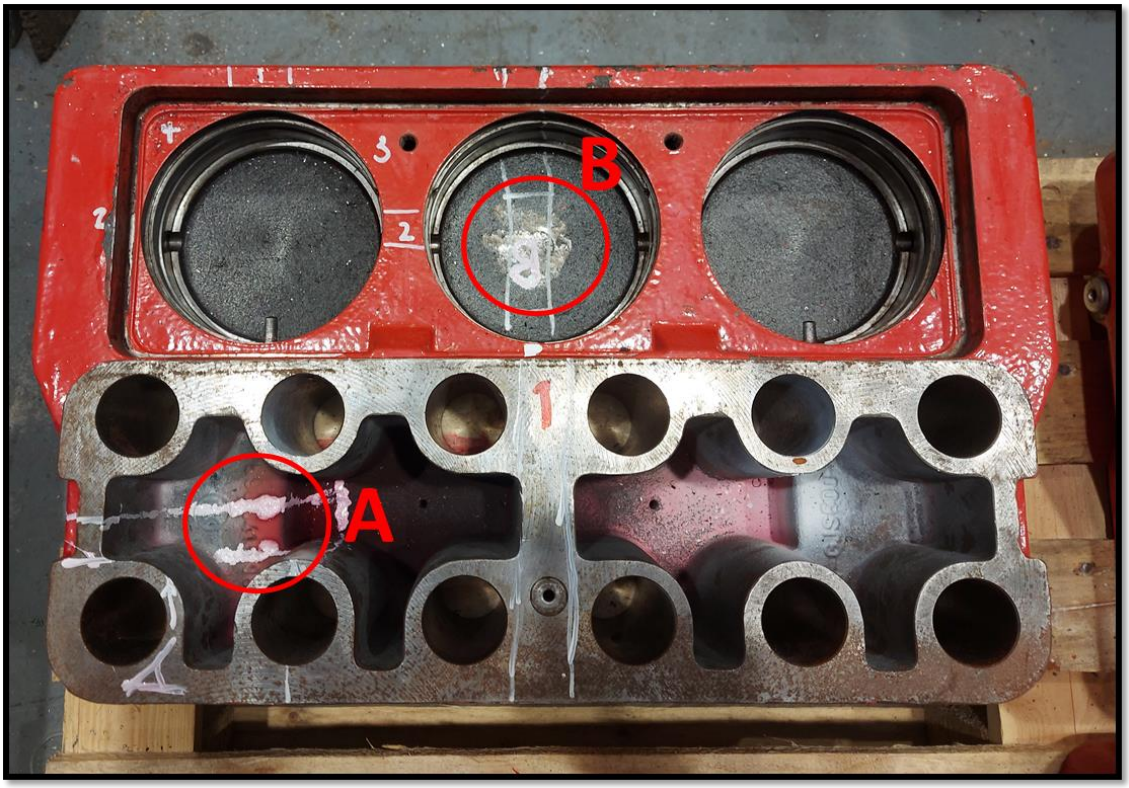

Figure 41: Locations Where Samples A & B Were Harvested From

The material was cut via band saw to create small sections and then added to a Bakelite sample moulds. They were then polished to mirror finish via a number of different grades of abrasive papers and finally a number of different grades of diamonds pastes. The sections were then etched before being examined under an optical microscope, see Figure 42.

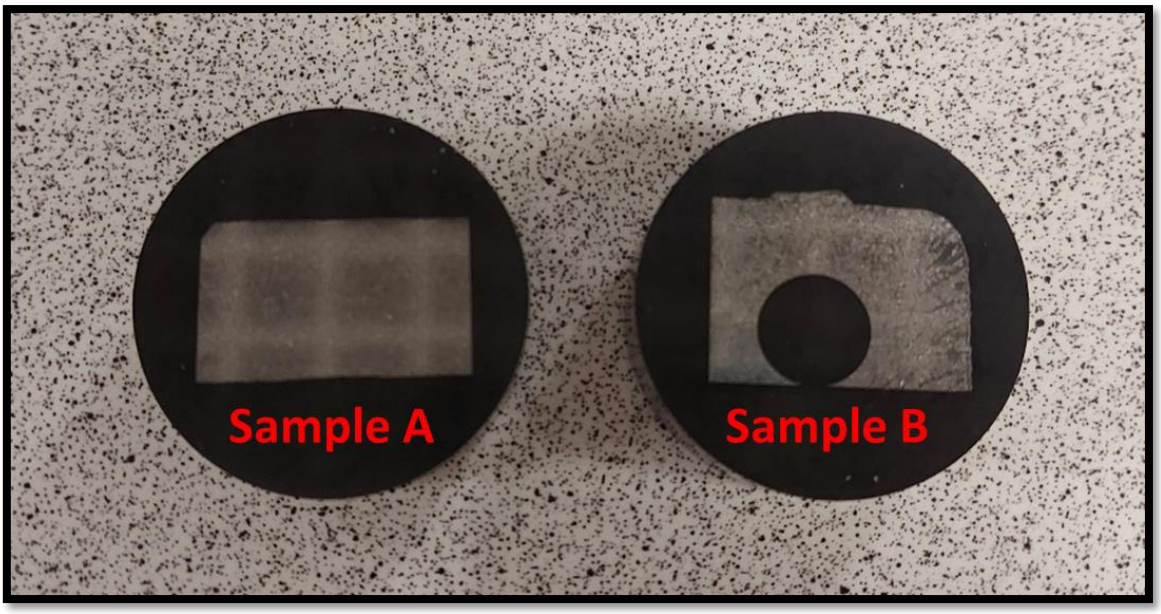

Figure 42: Metallography Samples Taken From the Caliper Yoke

3.5.2 Microscopy Analysis

Microscopic analysis was carried out on both samples with the surface layers the area of interest for both. As stated in BS ISO 1082:2018 the general structure in both the samples was a mixture of pearlite and ferrite, see Figure 43. From this it can been seen that the graphite is in spherical form which will decreased the risk of crack formations compared to flake graphite form. The ferrite, in white/ light grey, can be seen to form round the graphite with the pearlite forming around the ferrite.

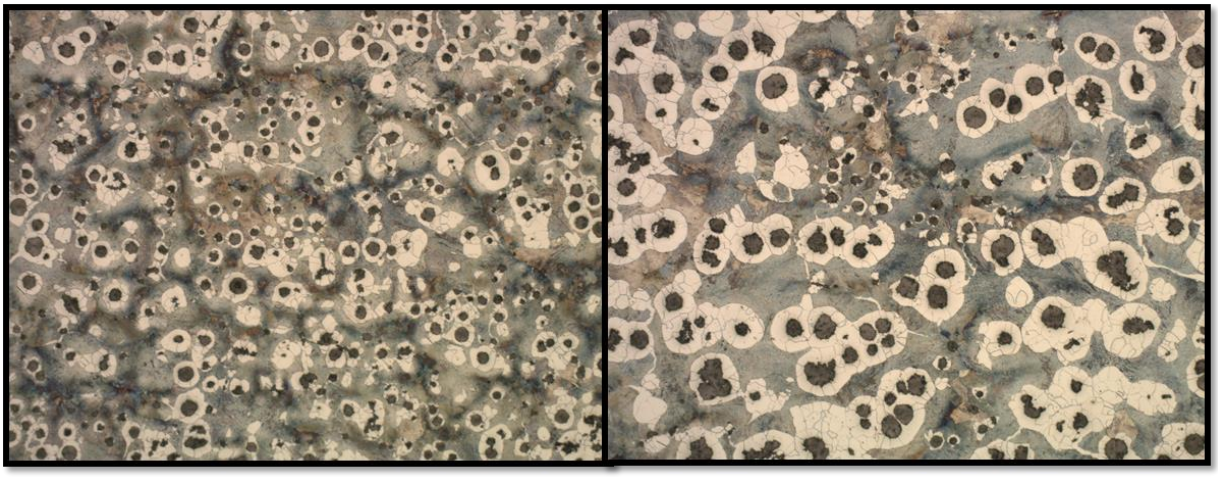

Figure 43: General Microstructure at x50: Left Sample A, Right Sample B

3.5.2.1 Sample A

Both the untouched surface and grounded surface were looked at to compare the effects of grounding casting defects. From a magnification of x50 it can be seen that at the cast skin the

composition of the material has changed to that of the body with more ferrite and a reduction in pearlite, see Figure 44. There is no sign in the grounded surface having any sort of material property change.

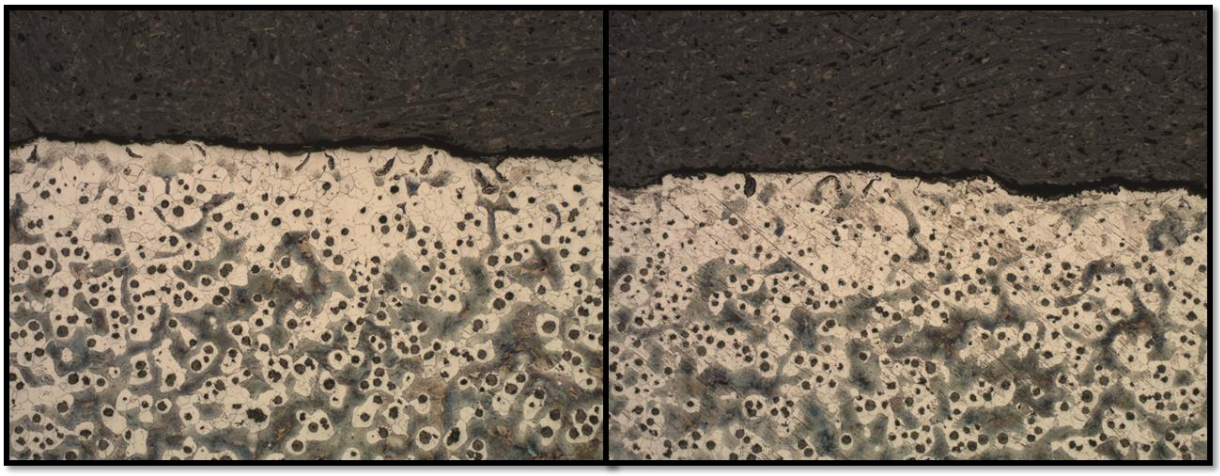

Figure 44: Bore Surface at x50: Left - Untouched Cast Skin, Right - Grounded Cast Skin

When looking at a higher magnification of x200 it can be seen that the grounded surface is more flatten compared to the normal surface and there is evidence of the surface being pulled to the left (highlighted in red), see Figure 45. What is also notable is the change in form of the graphite from spherical to flake. Overall there is little affect to the properties of the material from the grinding process. There is evidence of scarring but this is suspected to have little effect of performance. The most interesting observation was the change in structure closer to the cast surface.

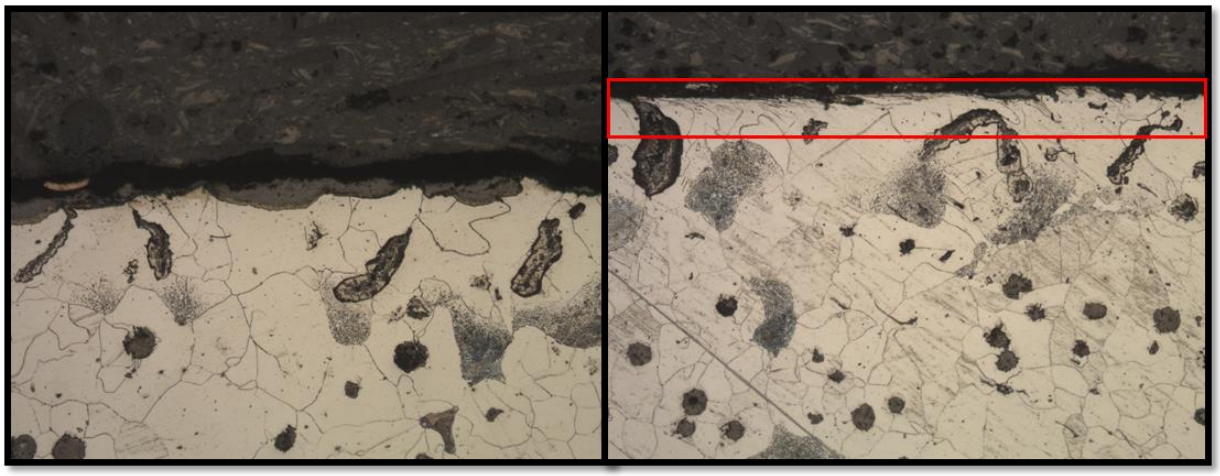

Figure 45: Bore Surfaces at x200: Left – Normal Untouched Surface, Right – Grounded Surface

3.5.2.2 Sample B

Sample B was analysed to find any evidence of fatigue cracking or possible causes. The main area of focus was geometry such as an internal hole, the embossed stamping and the casting surface. The first area looked at was the corner surface, see Figure 46, this showed the presentence of more flake graphite compared to that of the unground surface in the bores. No cracking was identified in this area.

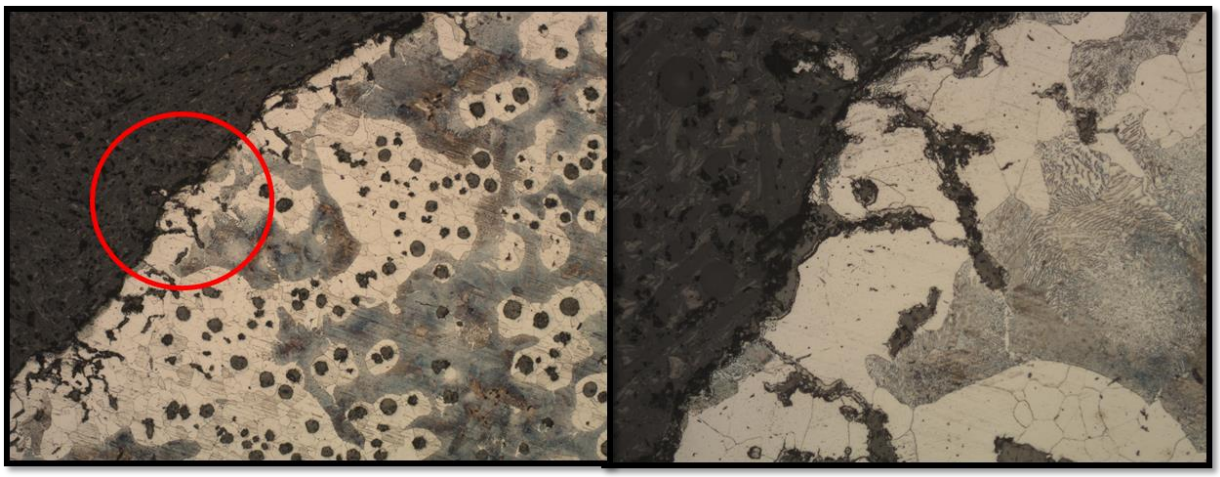

Figure 46: Corner Surface: Left – x50 with Area of Interest Highlighted in Red, Right – Area of Interest at x200

When looking at the internal hole the material structure around it was rich in pearlite, see Figure 47. This was to be suspected due to this being a machined feature through the main body of the component. Cracking is in area would be unlikely unless casting defects where present, which in this case they were not.

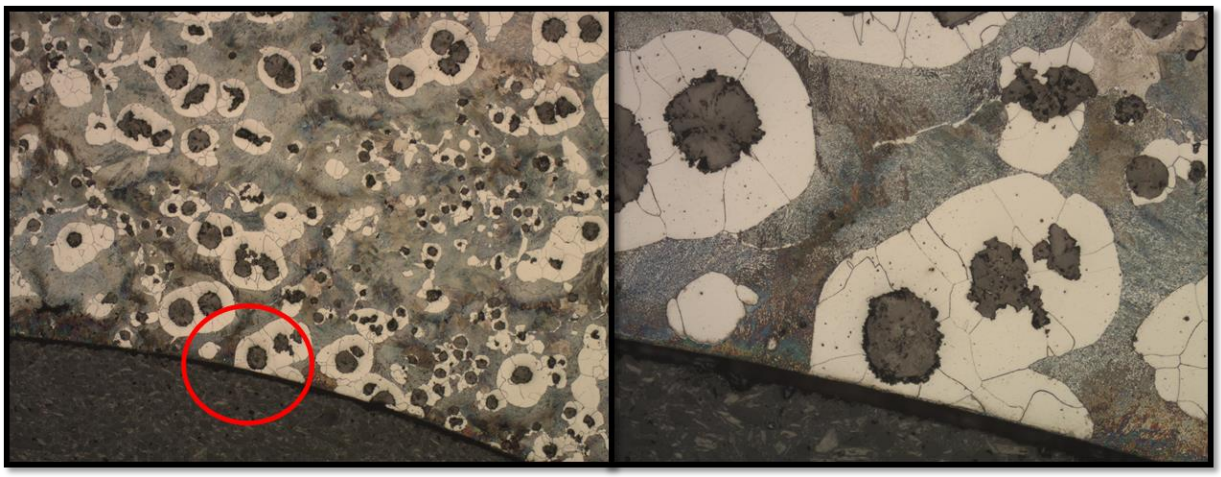

Figure 47: Internal Hole: Left – x50 with Area of Interest Highlighted in Red, Right – Area of Interest at x200

When looking at the embossed area it was clear again the difference in the cast skin layer to that of the main body, see Figure 48. Flake graphite was heavily present with areas having

graphite in a perpendicular direction to the surface. These areas are prime location for the formation of fatigue cracking as an easy access route into the materials structure. The corner at the start of the stamp was hard to see but as this would likely be an area on high stress concentration it was examined further via Scanned Electron Microscopy (SEM).

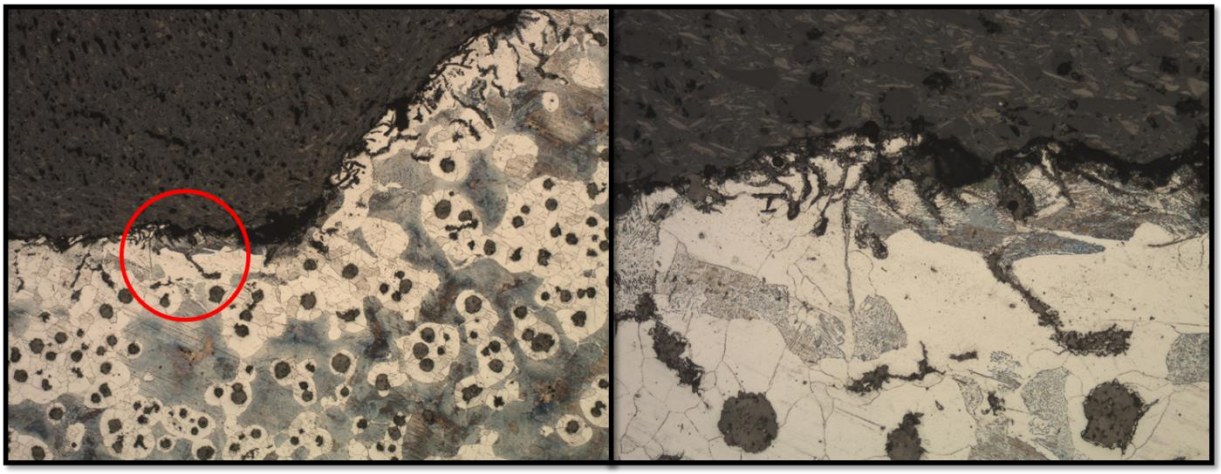

Figure 48: Beginning of Embossed Stamping: Left – x50 with Area of Interest Highlighted in Red, Right – Area of Interest at x200

The lowest quality of the cast skin was found at the side surface of the sample, see Figure 49, which is the exposed vertical cast surface inside the cavity. Surface roughness was clearly high and more flaking was present compared to that in the embossed surfaces. An anomaly was spotted in the material which seemed to have penetrated the material surface. This was suspected to be a grain of sand from the casting process but due to the limitation of optical microscopy a conclusion could not be made. As a result, this area was also examined further via SEM.

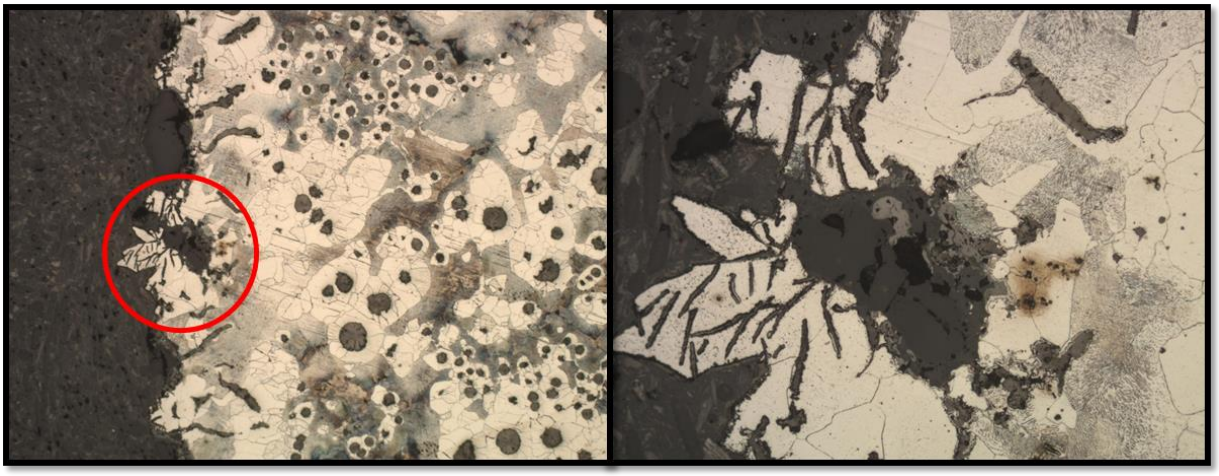

Figure 49: Side Surface: Left – x50 with Area of Interest Highlighted in Red, Right – Area of Interest at x200

3.5.3 Scanning Electron Microscope Analysis

SEM is the process of using electrons to view materials at a greater magnification than that of optical microscopy. This is due to optical microscopy being limited by the wavelength of the visible light spectrum in terms of resolution. SEM operates by firing electrons, which are guided through magnetic lenses, onto a surface where they penetrate it by a few microns. This releases secondary electrons as well as backscatter electrons and x-rays; these are utilised by a detector in order to create an image of the surface [31]. These signals also provide a useful insight to the material's composition by identifying what elements are present. This process does not provide exact compositional quantities but rather an indication of what elements are present at specific locations.

SEM was carried out to identify the composition of the anomaly seen at the side surface of Sample B as well as looking at the corner to evaluate if corrosion was occurring. Inspection was carried out via a Hitachi S3700-N SEM with an Oxford Secondary Detector, see Figure 50.

Figure 50: SEM Setup at the Advanced Materials Research Laboratory (AMRL) in the University of Strathclyde [32]

The sample was attached to a test stand via a conductive material. This conductivity was reinforced by adding a piece of copper tape between the sample and the stand. The stand and

sample height was measured to configure the SEM and placed into the chamber where all air was removed to create a vacuum.

The first area looked at was the embossed corner area, see Figure 51. Graphite (White) was detected at point 1. Points 2 and 3 showed the presentence of silica oxide (Yellow), also known as sand. This was surprising as it was not expected that sand particles would be present in this area. At points 4 and 5 Iron Oxide (Orange) was present this means that corrosion of the material has begun on the surface. This can weaken the material and can be utilised for crack initiation and growth. Flake graphite normal to the surface can be seen here as well; which can further entice growth due to the orientation as slip plane deformation occur normal to the surface during the early stages of a cracks life.

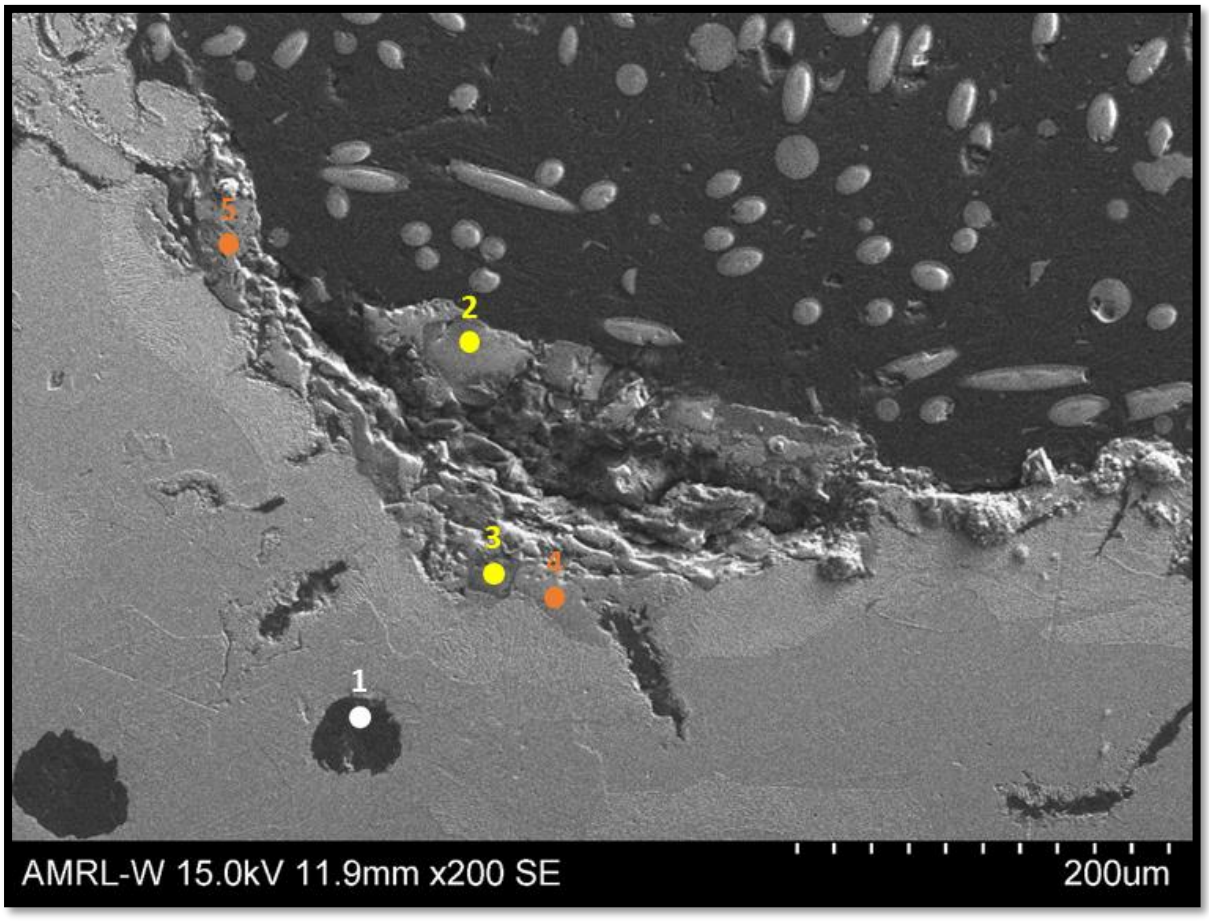

Figure 51: Embossed Stamp Corner at x200

The side surface was investigated next. This confirmed the theory that sand grains were present in the material as highlight in points 1 – 3 in Figure 52. Iron oxide was noted at points 4 and 5 which present a similar pattern to that seen at the corner of the embossed stamp with corrosion

occurring around sand grains. Point 6 is Bakelite (Black) and was measured to compare to other areas of the material.

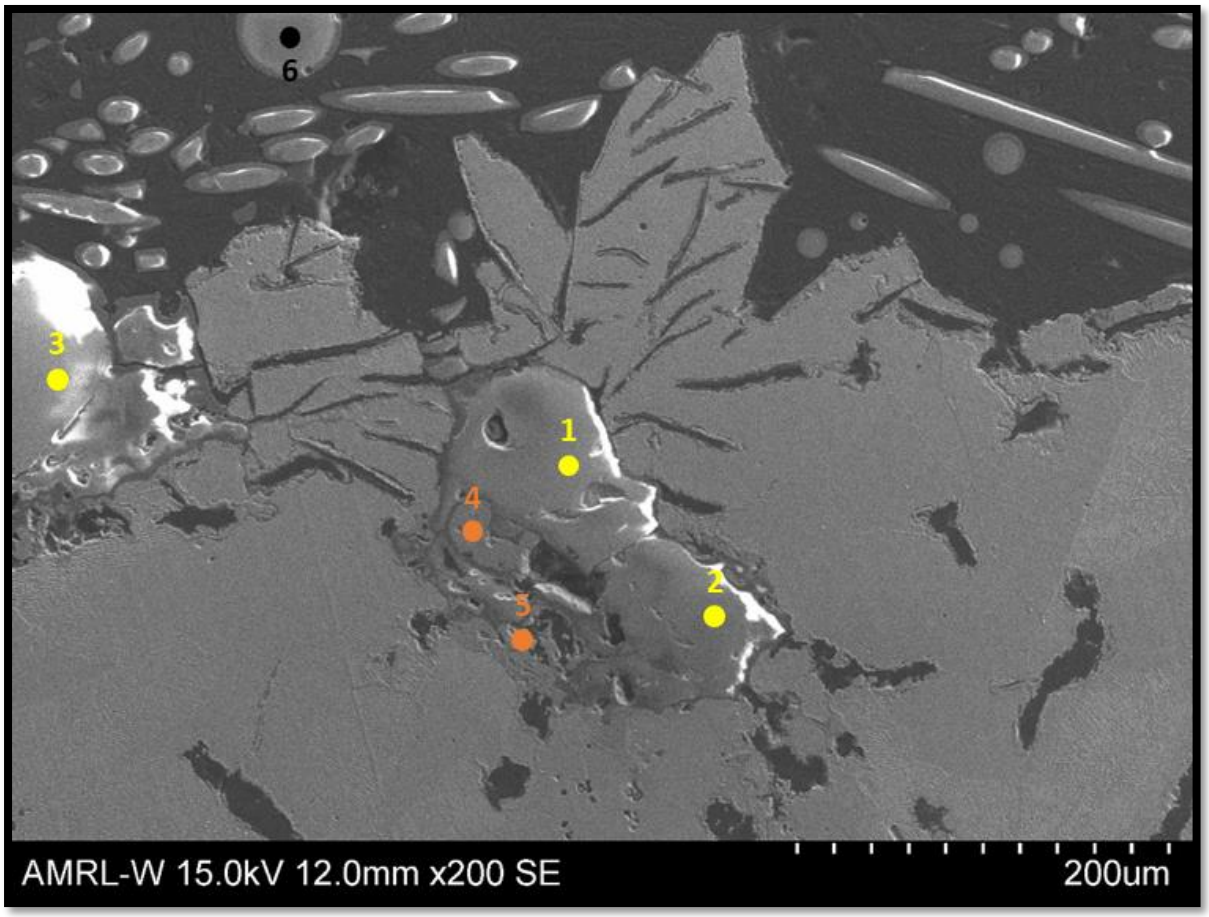

Figure 52: SEM Image of Suspected Sand Grain on Side Surface x200

Looking closely at the opening of where the sand grain is was discovered that the Bakelite material had flown into the opening, see Figure 53. This highlights a potential area where cracking could begin. With iron oxide present within the material surface this can provide a route for cracking initiation into the material.

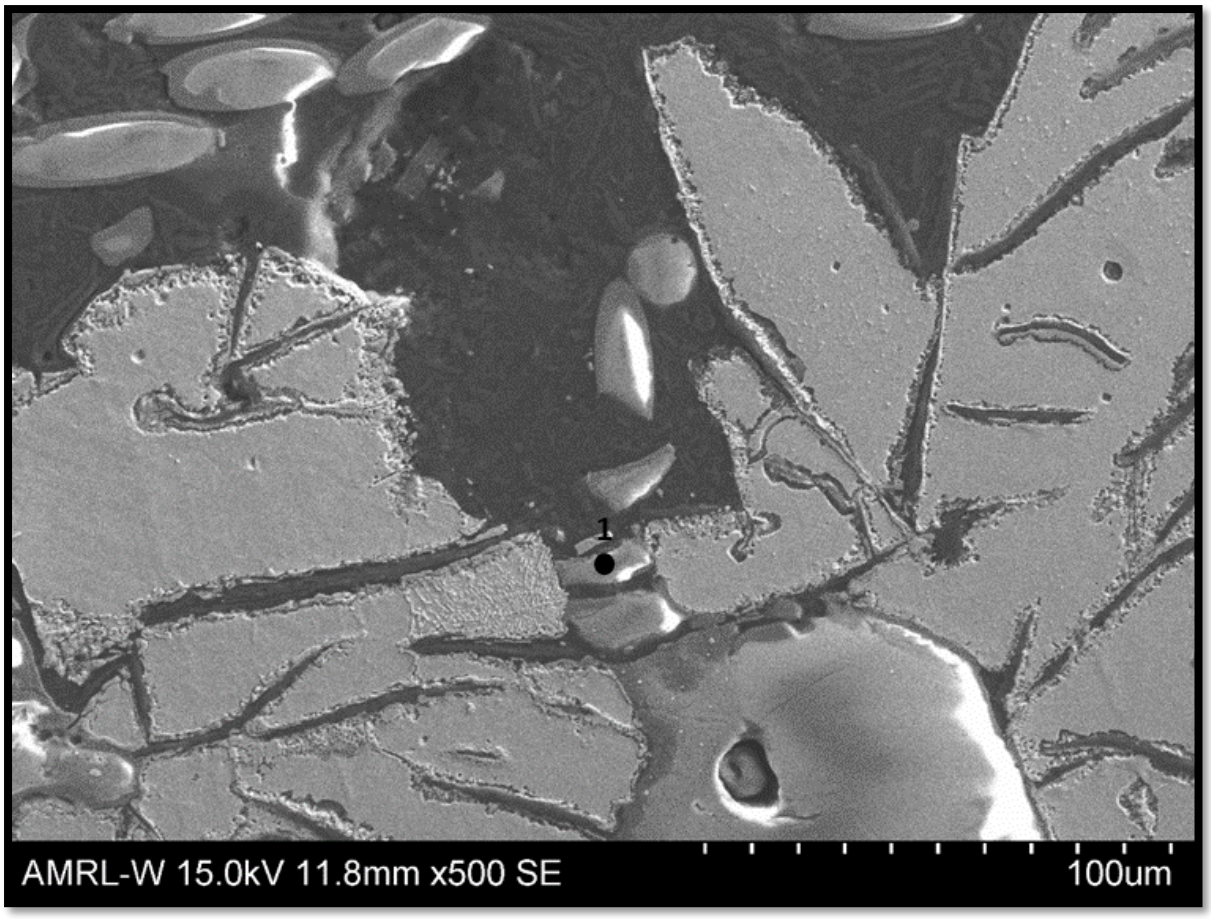

Figure 53: Side Surface Next to Suspected Sand Grain at x500

Figure 54 details a view of the two suspected sand grains found during microscopy. Points 2-4 reinforce earlier imagery that these areas are silica oxide. Point 1 shows the extent of which the iron oxide is present at this location in the material. Point 5 was found to be Bakelite. This is another example of there being openings formed between the material surface and the sand. This surface geometry is again an opportunity for cracks to form and work through the weaker flake graphite present in the cast skin before propagating through the material.

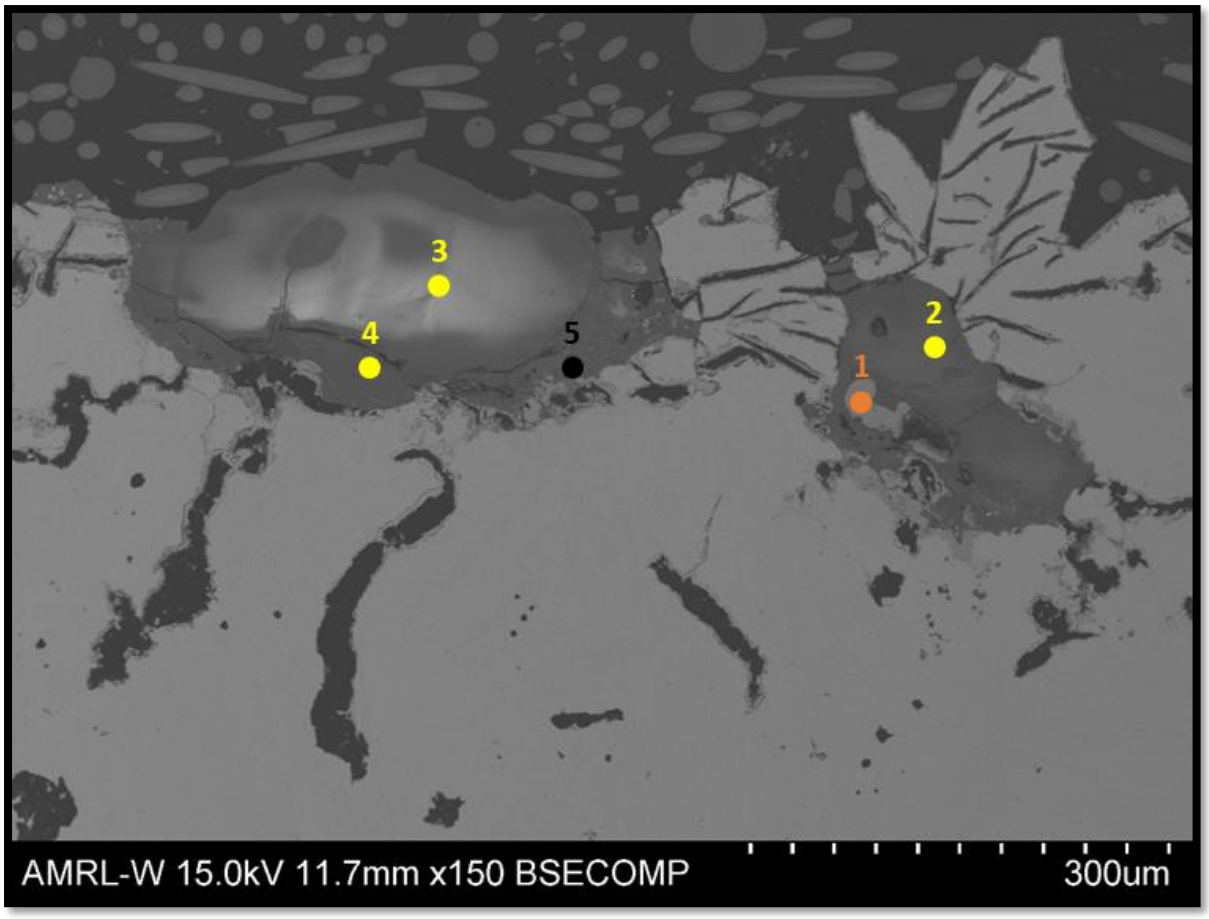

Figure 54: Side Surface Showing Both Suspected Sand Grains at x150

3.6 Fatigue Test Setup

A fatigue test setup has been designed in order to measure the effects of fatigue cracking on a caliper half; with loading conditions trying to replicate those seen in service within a lab environment. The benefit of this will be to show whether or not the simulation models has provided an accurate estimate of fatigue life and the location of failure points. It will also allow for an estimate of fatigue life based on crack sizing to be given during inspection. This knowledge will enable a point of no return for the calipers to be set. Where they will be deemed either unsafe or uneconomical viable to go back into service. Unfortunately, due to project time constraints and resource availability the project was unable to manufacture and carry out the experiment.

3.6.1 Fatigue Fixture Design

The design is based around the Instron 8802 fatigue testing machine which produces a loading force of 250kN. This was chosen due to this being the largest fatigue tester within the department. The purpose of the fixture is to secure the caliper in place as loading and unloading

occurs for high cycle fatigue testing. To do this the Instron 8802 was modelled in Creo as per the manufactures specifications, see Figure 55.

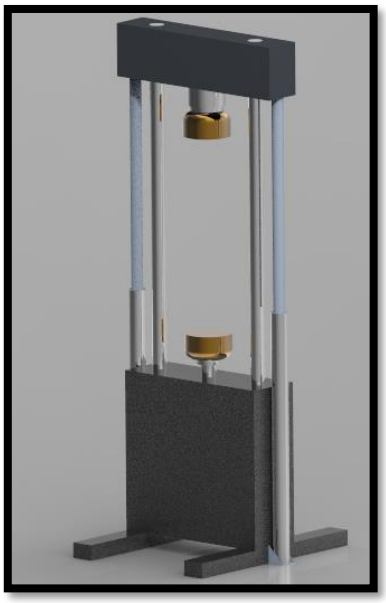

Figure 55: Instron 8802 CAD Model

The CAD model for the caliper was assembled in the model and positioned so that the top of the caliper was facing downwards to the bottom of the Instron, see Figure 56. This positioning was done due to the Instron working by having the top mount move into position with the hydraulic clamp at the bottom applying the force. Once the caliper was correctly positioned in the experimental "zero" position; which is the point were no load is applied, a frame was modelled around this and the Instron.

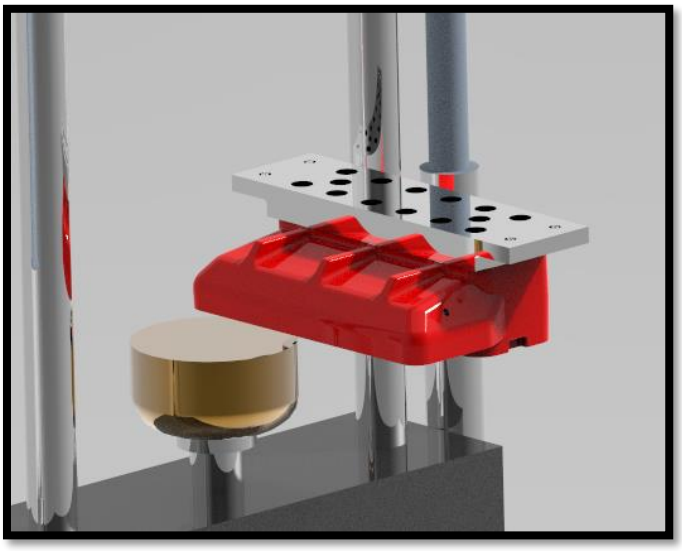

Figure 56: Instron Assembly with BSAB-S-120 at Zero Position

For the frame design to work in a cost effective manner and ensure the part is securely constrained two frames would need to be constructed with a mounting plate to hold the caliper. The two frames were designed to be the same to reduce manufacture and to be made of 50 x 50mm steel tubing cut and welded into shape. This material was picked due to its ease of manufacture, strength properties and low cost. The design allows for the frame to sit in-between the two feet of the Instron allowing for the positioning of the caliper. The top horizontal part of the frame is extended to the front to allow for the caliper corner to be positioned directly in line with Instron's hydraulic press axis, see Figure 57.

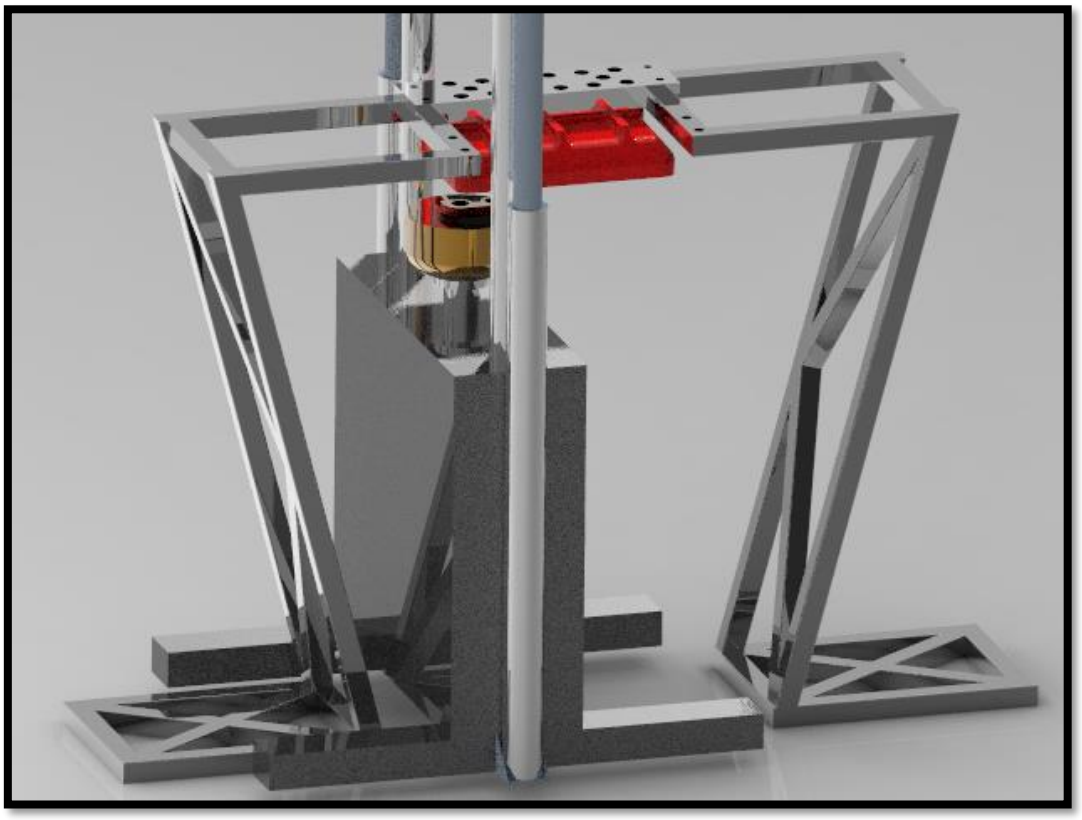

Figure 57: Instron Assembly with Mounting Frames

A set of four through holes are placed along the front of the extended section's tube. These are clearance holes to allow M20 bolts to past through and be secured via nuts on the opposite side, see Figure 58. As these will be the same on both frames it will not matter what position each are in avoiding any mounting confusion between frames.

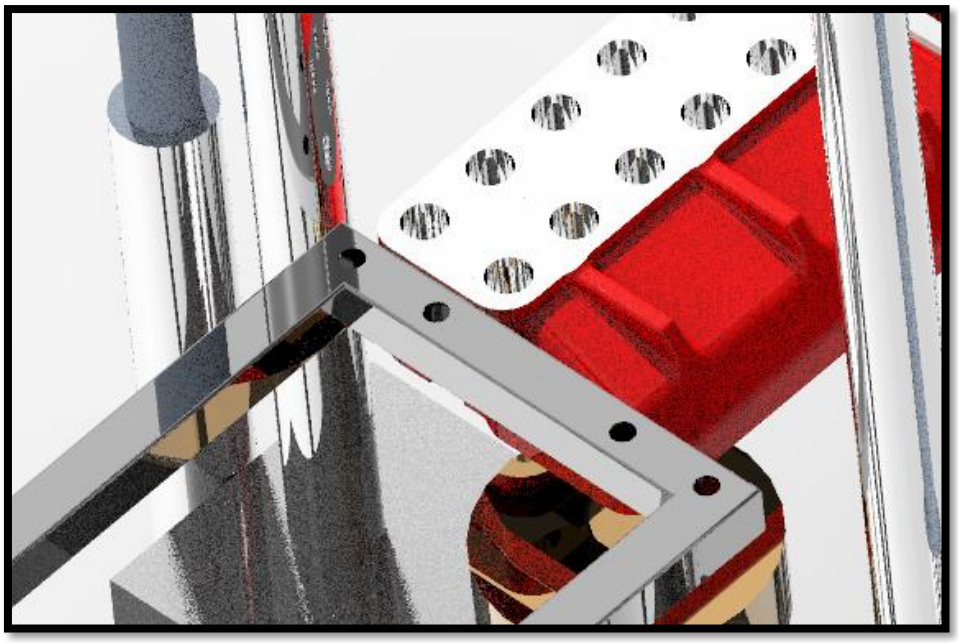

Figure 58: Mounting Frames Clearance Holes for Mounting Plate

At the bottom of the frame area has been left to allow for concrete blocks or slabs to be placed on top. This will act as a counter weight for the frame and allow the caliper to remain in position. Support beams have been added at angles to ensure the frame can take the load of the calipers and mounting plate, see Figure 59.

Figure 59: Mounting Frame Showing Supporting and Concrete Counter Weight Blocks

A mounting plate has been designed that is 80mm thick with two mounting surfaces at each side to allow the plate to fit on the frames. The hole pattern is the same as the caliper and are M36 x 3 through threads. Eye bolts have been added to allow for easy handling of the mounting plate and caliper as one unit, see Figure 60.

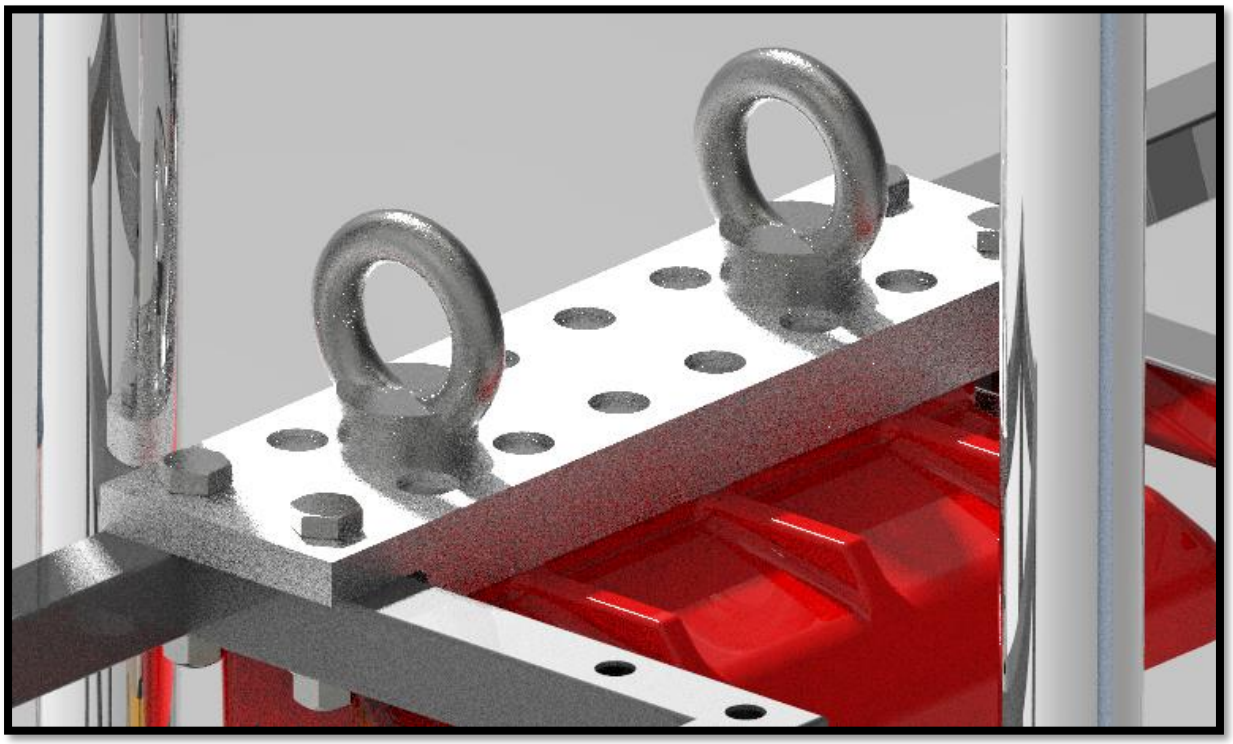

Figure 60: Mounting Plate with Eyebolts for Lifting

3.6.2 Experiment Operations

The part has been quoted by Svendborg to withstand 1.5 million cycles. The experiment will be carried out at the Instron's maximum force of 250kN until failure. To measure fatigue growth, the part will be inspected via a Non-Destructive Testing (NDT) method. This will take place before the start of the experiment where after it will occur every 20,000 cycles until crack initiation has begun and is past in the cast skin. Once past the cast skin the part will be inspected every 50,000 cycles. This is due to the crack front moving faster in the initiation period after which the crack growth rate will slow as the material has moved past the weaker cast skin to the material bulk. At this point in the propagation the crack will be determined by the initial resistance i.e. fracture toughness of the material. Crack monitoring should be carried out via a non-destructive test (NDT) method. Further work will need to be carried out to incorporate this to the fatigue test design. At the University of Strathclyde both the Advanced Materials Research Laboratory AMRL and Centre for Ultrasonic Engineering (CUE) have the necessary equipment and skillsets to design this portion of the experiment.

3.7 Fatigue Test Specimens

Fatigue test specimens were harvested from the caliper at various locations, see Figure 61. This was to carry out fatigue testing as per ASTM E606, Standard Test Method for Strain-Controlled Fatigue Testing, in the hope to evaluate the material's fracture toughness and create a S-N curve. The fracture toughness of the material will allow for the component's remaining life to be calculated based on the dimensions of a propagating crack. The S-N data will allow for more accurate modelling to be done and give a better understanding of the materials properties. Unfortunately, due to the nature of the testing and time constraints of this project phase the testing was not performed but test specimens have been prepared and are ready for the next phase of the project, drawings for these can be found in Appendices 6-8.

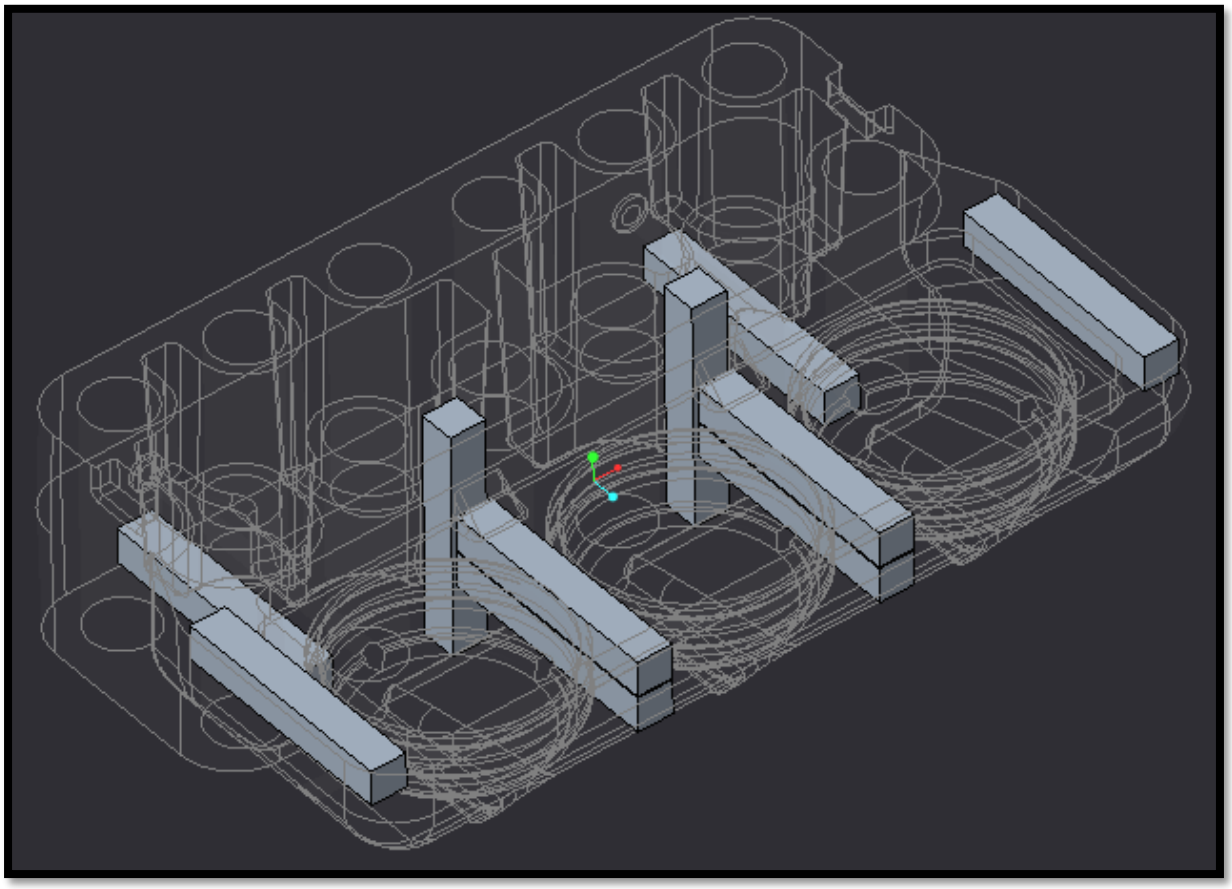

Figure 61: Fatigue Specimen Locations Harvested from BSAB-S-120

4.0 Conclusions

This phase of the project mainly focused on the fatigue within the calipers. However, it is evident that within the bores three main areas of concern have been found and should be investigated further:

- Side loading is effecting the form of the hydraulic cylinders. Manufacturing tolerances for concentricity and position could not be found and therefore impact of this to performance is unknown.

- Wear is occurring at the bottom of the cylinders; removing the cast surface. This could be a result of hydraulic fluid flow or oil contamination corroding the cast surface. This should be investigated further to see how this is affecting the braking performance.

- Leaking of seals has been reported and could be a result of oil contamination. Seal damage will affect the performance of the parts and impact operation and maintenance costs. Samples of oil from out of service components would prove beneficial.

Looking at the fatigue cracking in the component FEA simulations suggest that the area in the cavity between the holes is the last place the component is likely to fail. This is the thickness part and is secured via the 12 mounting holes. Loading 1 scenario was similar to that done by Siemens and suggests that the loading is uniformly distributed across the braking surface. However, it is clear this is not the case; with the braking pads showing uneven wear. This could be a result of the first cylinder in the hydraulic sequence being activated and taking more of the load compared to the other pistons. This would create torsion within the part. Loading 2 shows that when a load is applied to only one end, that the part experiences torsion and fatigue cracking is likely to occur on the ledge surface within the cavity. However, under Loading 2 this area would be the last to fail.

Apart from the bottom of the piston cylinder, the cavity area is the only area of the caliper that is not machined or painted and is the only surface the cast skin open to the external environment. When looking at the microscopy of the components Sample A has a better surface roughness to that of Sample B. Both samples have a cast skin which has a lower fatigue strength compared to the bulk material. When looking at the microstructure flake graphite is seen in the

skin which is more subjectable to cracking due to its form. Sample B also showed sand grains being stuck to or into the surface of the cast skin with iron oxide underneath. This could be a result of oxygen being trapped in between the grain and surface causing corrosion to start.

As a result of the ledge surface having a high surface roughness with evidence of corrosion starting this is a perfect area for fatigue cracking to initiate. The cast skin having high volumes of flake graphite will cause an easy pathway for a crack front to propagate into the material. The stamping location will also have an affect with stress concentrations at the embossed corners increasing risk of crack initiation. These factors combined with a loading condition causing torsion in the part would explain why fatigue is occurring in this area.

For life estimates NDT testing can we used to identify and measure any cracking on the part. If the cracking has reached the propagation stage; using the material's fracture toughness and environmental condition the remaining cycles can be estimated. These should be based on maximum stress ranges to ensure worst case scenarios are considered.

4.1 Recommendation for Next Phase and Life Extension of Calipers

From this project the following recommendations are made in an effort to extend the life of calipers:

- Information on geometrical tolerances should be secured from the manufacture to assess if the bores are out of tolerance or not. Geometrical tolerances are more accurate and restricting than those on dimensions.

- If bores are out of tolerance, then a possible solution could be to re-bore the piston cylinders to accommodate seals at 125mm diameter. This will ensure effects of side loading do not worsen or effect performance. This should be investigated further to assess impact on hydraulic performance.

- If oil contamination is found to be present in oil from in service units, then upgrading oil filtration systems may provide a solution. This will allow for smaller particles to be removed from the oil will help to stop system corrosion from metal particles and other contaminates.

- If crack initiation has started within the cavity surfaces but has not begun to propagate into the material the cast surface in this area should be removed. This could be done via a process such as sand blasting. This will remove the weak cast surface layer and avoid cracking into the bulk of the material. It is also recommended that a surface protection coating is applied to reduce risk of corrosion after the removal of this surface. This could be either via paint or a chemical conversation coating as they can be applied easily.

The following is a list of recommendations for the next phase of the project to look at in terms of fatigue analysis:

- Fatigue testing should take place in an effort to create an S-N curve for the material. This will enable better modelling to be carried out to determine what forces are experienced at the ledge surface during maximum loading.

- Fracture toughness should be measured to allow for fatigue life estimates to be made for propagating cracking. This will need to be combined with FEA modelled to determine maximum forces experienced by the crack.

- Fatigue experiments should be carried out as per detailed above. This will an excellent validation process to show if the cast skin and loading conditions are the influencing factors leading to component failure. It will also highlight any other issues that could impact component life extension.

- The effects temperature ranges within the nacelle have on the seals should to analysed to see if thermal fatigue is occurring and resulting in seal failure.

- A NDT method should be developed and incorporated into the design of the fatigue testing experiment to monitor crack growth from cyclic loading.

5.0 References

[1] The University of Strathclyde, “Strathclyde, SSE Renewables & Renewable Parts sign joint MoU to develop a sustainable wind sector,” 15 June 2022. [Online]. Available: https://www.strath.ac.uk/whystrathclyde/news/2022/strathclydesserenewablesrenewablepartssignjointmou/. [Accessed 12 July 2022].

[2] D. P. D. Modica, “Embarking on Sustainable Decommissioning.,” July 2022. [Online]. Available: https://www.linkedin.com/posts/renewable-parts_sustainable-decommissioning-leaflet-activity-6953373642399375360-etrn?utm_source=linkedin_share&utm_medium=member_desktop_web.

[3] Renewnable Parts Ltd, “About,” Renewable Parts Ltd, 2022. [Online]. Available: https://www.renewable-parts.com/about.

[4] Siemens, “G4 Yaw Brake Caliper- Structural,” Siemens, 2016.

[5] Hard Chorme Specicalists, “The History of Hydraulics,” Hard Chorme Specicalists, 29 October 2019. [Online]. Available: https://hcsplating.com/history-of-hydraulics/.

[6] RHK Hydraulic Cylinder Services Inc., “Hydraulic Cylinder Failure: 7 Common Causes,” 2022. [Online]. Available: https://rhkhydraulics.com/blog/hydraulic-cylinder-failure-7-common-causes/. [Accessed 25 03 2022].

[7] Fluid Power World, “Hydraulic cylinder problems: Side loads,” 2022. [Online]. Available: https://www.fluidpowerworld.com/how-do-hydraulic-cylinders-fail-side-loads/. [Accessed 24 05 2022].

[8] Gianni Nicoletto and Tito Marin, “Failure of a heavy-duty hydraulic cylinder and its fatigue re-design,” *Engineering Failure Analysis,* vol. 18, pp. 1030-1036, 2011.

[9] Asad Hameed, Ali Nawaz, Haris Ali Khan, Zahid Mehmood and Farooq Akram, “Failure analysis of a cracked cylinder block assembly of an aircraft,” *Engineering Failure Analysis,* vol. 113, 2022.

[10] Inspire Clean Energy , "Who Discovered Wind Energy?," Inspire Clean Energy , 7 October 2016. [Online]. Available: https://www.inspirecleanenergy.com/blog/clean-energy-101/who-discovered-wind-energy.

[11] Søren Stubkier, Henrik C. Pedersen, Torben O. Andersen and Kristian Markussen, "State of the art-hydraulic yaw systems for wind turbines," in *Conference: Proc. 12th Scandinavian International Conference on Fluid Power*, 2011.

[12] M. H. H. Albadi, "On Techno-economic Evaluation of," Researchgateway, Ontario, 2010.

[13] Gerardo Lumagbas Augusto, Laurence A. Gan Lim and Alvin B. Culaba, "Design of Yaw Brake System for Horizontal Axis Wind Turbine Generator," The Instiute of Electrical and Electronic Engineers Inc, Manila, 2015.

[14] J. Schijve, Fatigue of Structures and Materials, Delft: Springer, 2009.

[15] Siemens, "What is a SN-Curve?," 19 August 2019. [Online]. Available: https://community.sw.siemens.com/s/article/what-is-a-sn-curve . [Accessed 26 July 2020].

[16] PP Benham, RJ Crawford and CG Armstrong, Mechanics of Engineering Materials, Belfast: Pearson, 1996.

[17] Wermac, "Dye Penetrant Inspection," Wermac, 2022. [Online]. Available: https://www.wermac.org/others/ndt_dyepenetrant.html.

[18] Code of Steel Industrial Inspections, "PT (Dye Penetrant Testing) LVL I & II," Code of Steel Industrial Inspections, 2022. [Online]. Available: https://www.codesteel.com/pt-dye-penetrant-testing-lvl-i-ii/.

[19] E. Mohseni, "Ultrasound Testing Slide Pack," University of Strathclyde, Glasgow, 2022.

[20] E. Mohseni, "Eddy Current Testing Slide Pack," University of Strathclyde, Glasgow, 2022.

[21] Material Properties, “What is Radiography Testing Definition,” Material Properties, 2022. [Online]. Available: https://material-properties.org/what-is-radiography-testing-definition/.

[22] ASM International, “Fatigue and Fracture Properties of Cast Irons,” *ASM Handbook,* vol. 19, pp. 665-679, 1996.

[23] MártonGróza, YvesNadot and Károly Váradi, “huFatigue design of cast iron components with surface discontinuities,” in *MATEC WEB of Conferences*, Budapest, 2018.

[24] Sarum Boonmee and Doru M. Stefanescu, “The Mechanism of Formation of Casting Skin in CG Iron and its Effect,” *Key Engineering Materials,* vol. 457, pp. 11-16, 2010.

[25] Kim Bergner, Jan Hesseler and Christoph Bleicher, “Fatigue analysis of cast iron components considering the influence of casting skin,” *Structural Intergrity Procedia,* vol. 19, pp. 140-149, 2019.

[26] Kim Bergner, Christoph Bleicher and Rainer Wagener, “Influence of remaining casting skin on the fatigue strength of cast iron components,” *25th International Conference on Fracture and Structural Integrity,* vol. 18, pp. 792-801, 2019.

[27] Renewables Ninja , “Renewables Ninja,” Renewables Ninja , 2019. [Online]. Available: https://www.renewables.ninja/.

[28] NASA, “What are Newton's Laws of Motion?,” NASA, [Online]. Available: https://www1.grc.nasa.gov/beginners-guide-to-aeronautics/newtons-laws-of-motion/. [Accessed 11 07 2022].

[29] Svendborg, “Installation and Maintenance Manual Hydraulic Active Disc Brake BSAB120-S-200 with Stepseal,” Svendborg, 2016 .

[30] Jens Bergstr€om, Christer Burman, Jonas Svensson, Andreas Jansson, Charlotta Ivansson, Jing Zhou and Sima Valizadeh, “Very High Cycle Fatigue of Two Ductile Iron Grades,” *Steel Research International,* pp. 614-623, 2016.

[31] Nanoscience Technology, “Scanning Electron Microscopy,” Nanoscience Technology, 2022. [Online]. Available: https://www.nanoscience.com/techniques/scanning-electron-microscopy/.

[32] ULab, “ Scanning Electron Microscope (W-SEM),” ULab, 2022. [Online]. Available: https://www.ulabequipment.com/equipment.php?ID=1161.

[33] ALTRA Motion , “BSAB 120 | Svendborg Brakes,” 2022. [Online]. Available: https://www.altraptchina.com/zh-CN/products/heavy-duty-clutches-and-brakes/svendborg-brakes/hydraulic-brake-products/active-brake-products/bsab-120. [Accessed 24 April 2022].

[34] U.S. Energy Information Administration , “Wind explained Types of wind turbines,” 3 November 2021. [Online]. Available: https://www.eia.gov/energyexplained/wind/types-of-wind-turbines.php. [Accessed 21 07 2022].

6.0 Appendices

6.1 Appendix 1 – Mounting Data for BSAB-S-100 for Inside Mounting [29]

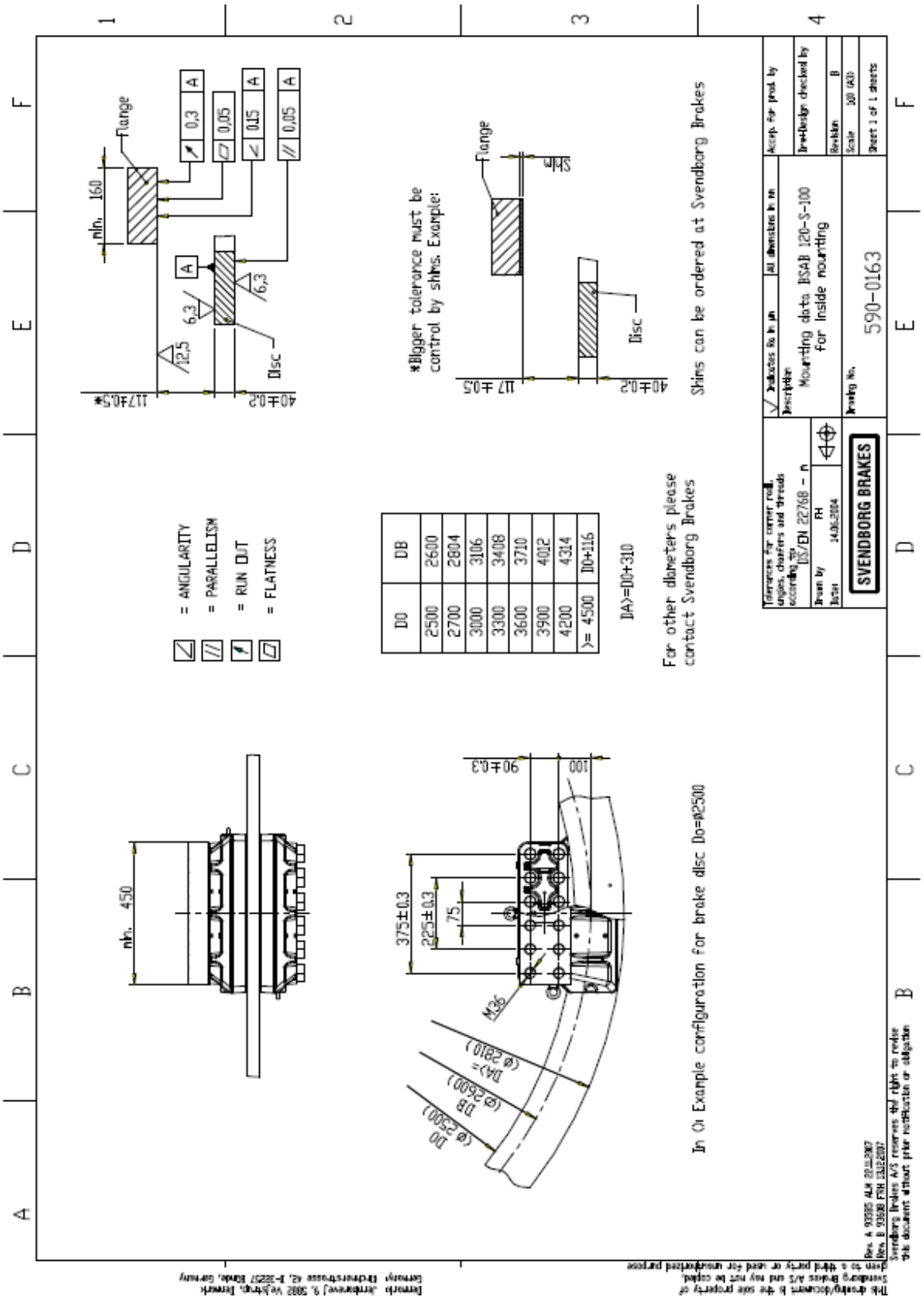

6.2Appendix 2 - BSAB 120-S-200 Half with Stepseal [29]

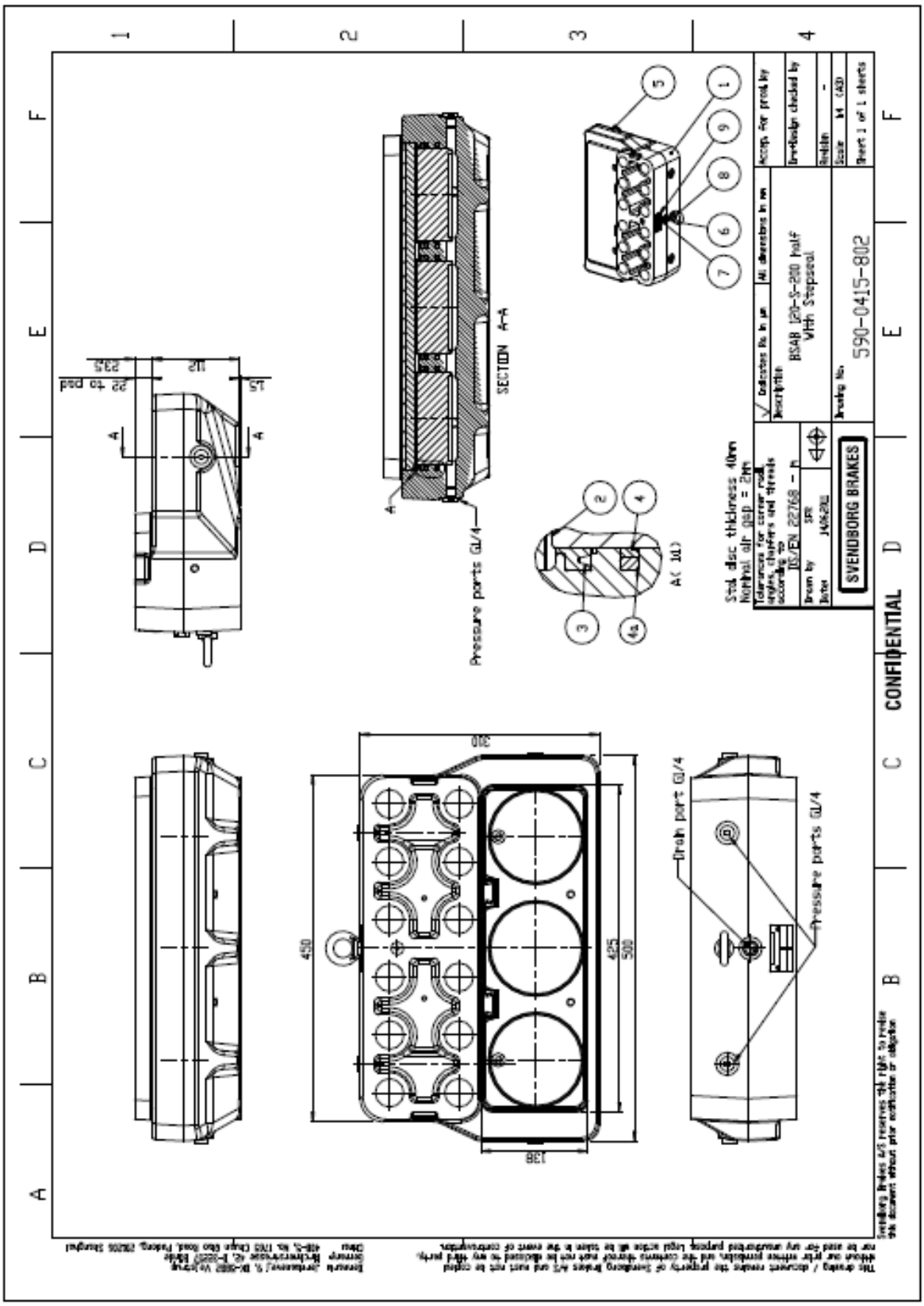

6.3Appendix 3 – BSAB-S-100 Drawing [33]

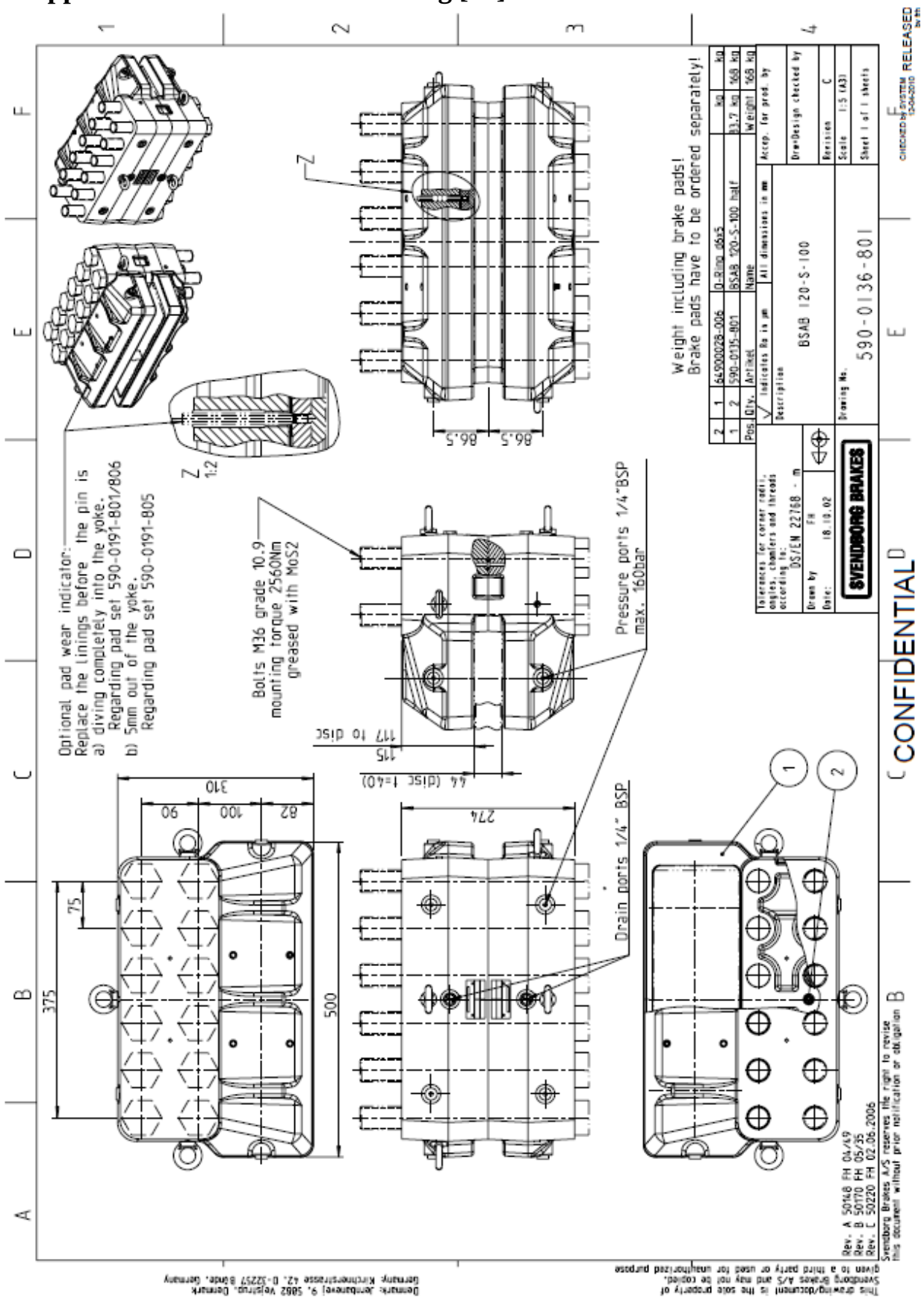

6.4 Appendix 4 - BS ISO 1083:2018 Material Properties

Table G.1 — Typical properties[a]

Characteristic	Unit	Material designation												
		ISO 1083/ JS/650-22	ISO 1083/ JS/400-18	ISO 1083/ JS/450-10	ISO 1083/ JS/500-7	ISO 1083/ JS/550-5	ISO 1083/ JS/600-3	ISO 1083/ JS/700-2	ISO 1083/ JS/800-2	ISO 1083/ JS/900-2	ISO 1083/ JS/450-18	ISO 1083/ JS/500-14	ISO 1083/ JS/600-10
Shear strength	MPa	315	360	405	450	500	540	630	720	810	—	nd[b]	—
Torsional strength	MPa	315	360	405	450	500	540	630	720	810	—	nd[b]	—
Modulus of elasticity E (tension and compression)	GN/m^2	169	169	169	169	172	174	176	176	176	170	170	170
Poisson's ratio ν	—	0,275	0,275	0,275	0,275	0,275	0,275	0,275	0,275	0,275	0,28 to 0,29	0,28 to 0,29	0,28 to 0,29
Compression strength	MPa	—	700	700	800	840	870	1 000	1 150	—	—	nd[b]	—
Thermal conductivity at 300 °C	W/ (K·m)	36,2	36,2	36,2	35,2	34	32,5	31,1	31,1	31,1	—	—	—
Specific heat capacity 20 °C to 500 °C	J/ (kg·K)	515	515	515	515	515	515	515	515	515	—	—	—
Linear expansion coefficient 20 °C to 400 °C	µm/ (m·K)	12,5	12,5	12,5	12,5	12,5	12,5	12,5	12,5	12,5	—	—	—
Density	kg/dm^3	7,1	7,1	7,1	7,1	7,1	7,2	7,2	7,2	7,2	7,1	7,0	7,0
Maximum permeability	µH/m	2 136	2 136	2 136	1596	1200	866	501	501	501	nd[b]	nd[b]	nd[b]
Hysteresis loss (B = 1T)	J/m^3	600	600	600	1345	1800	2248	2 700	2 700	2 700	nd[b]	nd[b]	nd[b]
Resistivity	µΩ·m	0,50	0,50	0,50	0,51	0,52	0,53	0,54	0,54	0,54	nd[b]	nd[b]	nd[b]
Matrix structure		ferrite	ferrite	ferrite	ferrite-pearlite	ferrite-pearlite	pearlite-ferrite	pearlite	pearlite or tempered martensite	tempered martensite or bainite[c]	ferrite	ferrite	ferrite

NOTE 1 1 MPa = 1 N/mm^2.

NOTE 2 Unless otherwise specified, the values given in this table come from measurements at room temperature.

a For details, see Reference [11].

b Not determined.

c For large castings, it can also be pearlite.

6.5 Appendix 5 – Project Phase 1 Stress Strain Curves

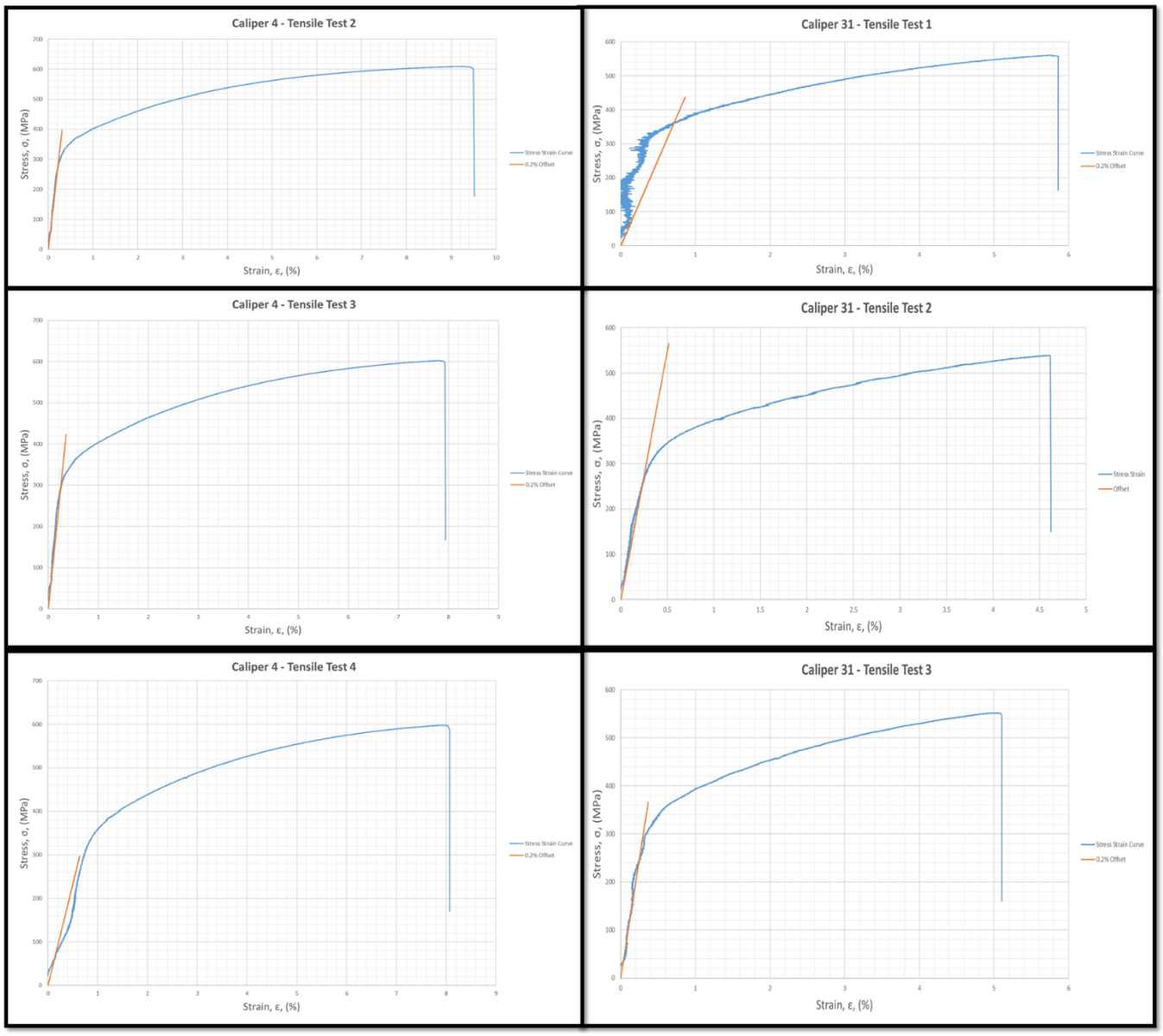

6.6 Appendix 6 – BSAB-S-120 FATIGUE SPECIMEN MACHINING

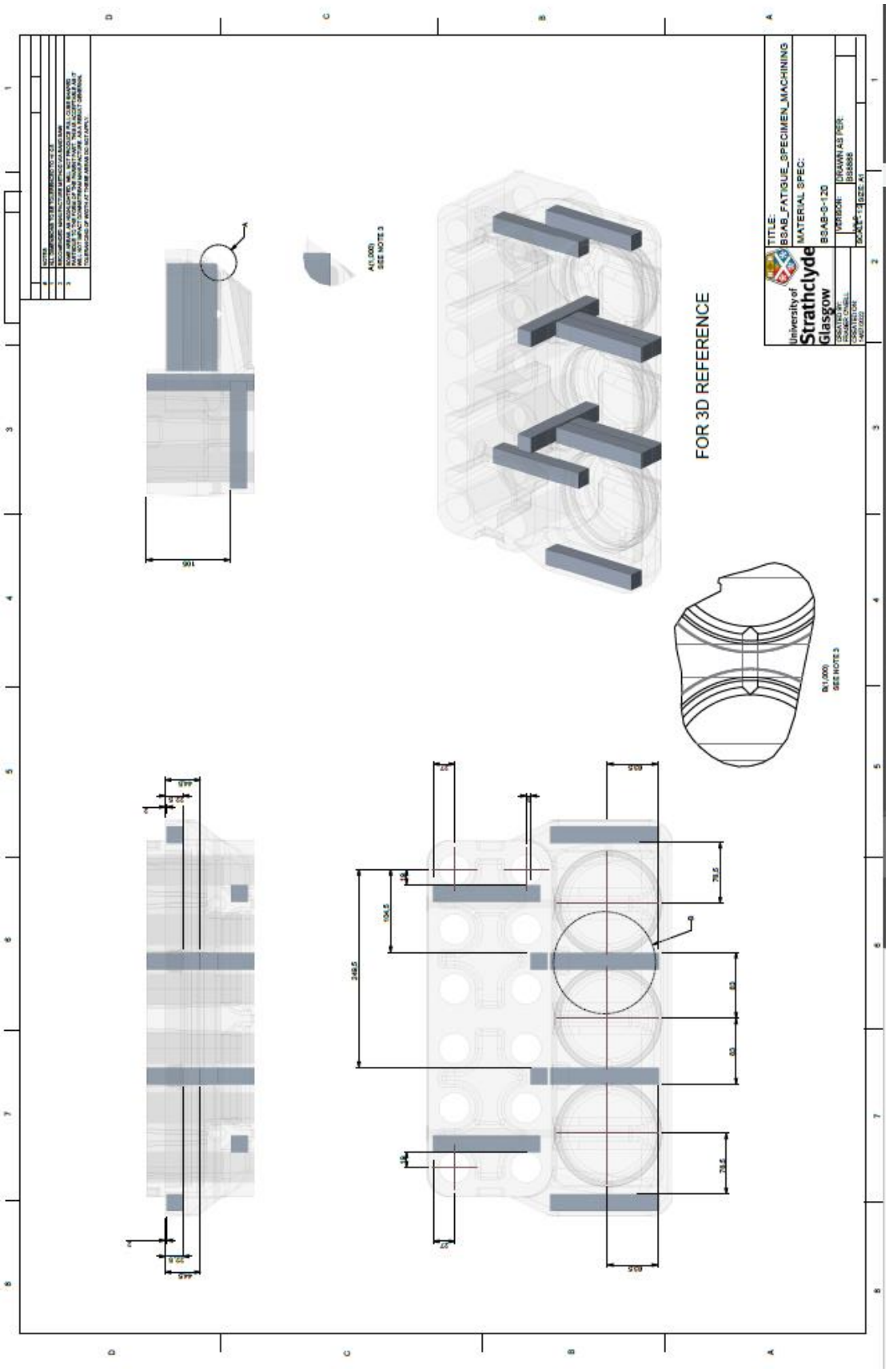

6.7 Appendix 7 – STAIN FATIGUE SPECIMEN SPACE CLAIM

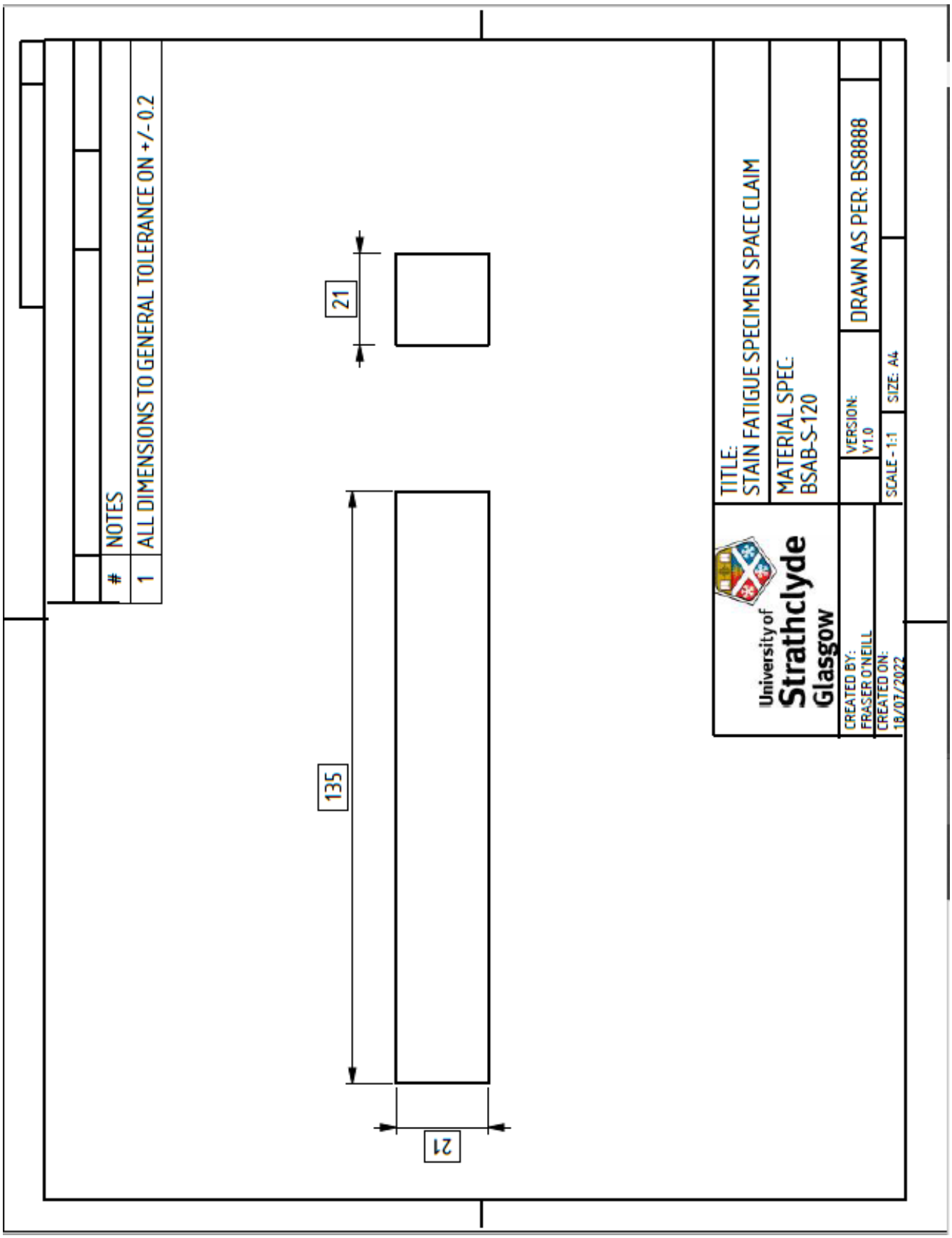

6.8 Appendix 8 – STAIN FATIGUE SPECIMEN